MODELING AND VALIDATION OF HITCHED LOADING

EFFECTS ON TRACTOR YAW DYNAMICS

Except where reference is made to work of others, the work described in this thesis is my own or was done in collaboration with my advisory committee. This thesis does not include proprietary or classified information

Paul James Pearson

Certificate of Approval:

Robert Jackson Professor Mechanical Engineering	David M. Bevly, Chair Assistant Professor Mechanical Engineering
Randy L. Raper Agricultural Engineer and Head Scientist, USDA/ARS National Soil Dynamics Lab Biosystems Engineering	Joe F. Pittman Interim Dean Graduate School

MODELING AND VALIDATION OF HITCHED LOADING EFFECTS ON TRACTOR YAW DYNAMICS

Paul James Pearson

A Thesis

Submitted to

the Graduate Faculty of

Auburn University

in Partial Fulfillment of the

Requirements for the

Degree of

Masters of Science

Auburn, Alabama
May 10, 2007

MODELING AND VALIDATION OF HITCHED LOADING

EFFECTS ON TRACTOR YAW DYNAMICS

Paul James Pearson

_____

Signature of the Author

_____

Date of Graduation

THESIS ABSTRACT

MODELING AND VALIDATION OF HITCHED LOADING

EFFECTS ON TRACTOR YAW DYNAMICS

Paul James Pearson

Master of Science, May 10, 2007
(B.M.E., Auburn University, 2004)

113 Typed Pages

Directed by David M. Bevly

This thesis develops a yaw dynamic model for a farm tractor with a hitched implement, which can be used to understand the effect of tractor handling characteristics for design applications as well as for new automated steering control systems. A model is found in which hitched implement conditions can be accounted for, and an improvement in yaw rate tracking prediction in both steady state and dynamic conditions is seen vs. traditional models. This model is termed the "3-wheeled" Front and Hitch Relaxation Length ("3-wheeled" FHRL) Model. Experimental data from a hitch force dynamometer are used to validate the way the hitched implement forces are derived in the "3-wheeled" FHRL Model and to determine if differential hitch forces can be ignored. Steady state and dynamic chirp data taken for a variety of implements at varying depths and speeds

are used to quantify the variation in the hitch parameter and to find the front and hitch relaxation length values. Finally, a model which accounts for four-wheel drive forces is derived, and experiments are taken which provide a preliminary look into the effect of four-wheel drive traction forces on the yaw dynamics of the tractor.

In comparisons with other traditional models, the "3-wheeled" FHRL Model is shown to be superior in its steady state yaw rate tracking ability with an RMS error of .245 deg/s vs. 1.96-2.07 deg/s for other models at a certain depth and also superior in its dynamic tracking ability with an RMS error of .675 deg/s vs. .748-1.37 deg/s for the other models. The experimental results from the hitch force dynamometer show that the implement performs according to the linear tire model and that the moment caused by differential forces at the hitch can be ignored. The hitch parameter, $C_{\alpha h}$, ranges from 452-3385 N/deg for various implements and depths tested in this thesis. The front tire relaxation length is found to be .37 m and the hitch relaxation length is found to be .4 m. The four-wheel drive experiments show that using four-wheel drive provided an increase in yaw rate from 9-21%, depending on the implement depth and speed.

ACKNOWLEDGEMENTS

I would first of all like to thank God for His wisdom and understanding. I would also like to thank Dr. Bevly and all of the current and past members of the GavLab- Matt Heffernan, Will Travis, Rob Daily, Evan Gartley, Randy Whitehead, Warren Flenniken, Rusty Anderson, Christof Hamm, John Wall, Kenny Lambert, Dustin Edwards, Wei Huang, Mike Newlin, Benton Derrick, Ben Clark, Matt Lashley, and David Hodo for their help, support, and companionship throughout the years.

I thank Deere & Co. for their support and donation of the use of the Deere 8420 and 8520 during this project. I also thank USDA and Dr. Randy Raper for the use of their dynamometer. Thanks to Eric Schwabb and Dexter LaGrand. Thanks go to Dr. Jim Bannon, and Bobby Durbin and all the folks at the EV Smith Research Station for their help and use of land for experiments. I would like to thank the gang back home for all of their support and love too- Mom, Dad, Jr., Sam, Katie, Sunny, Cody, Sissy, and Chad.

Style of Journal Used:

ASME Journal of Dynamic Systems, Measurement, and Control

Computer Software Used:

Microsoft Word 2003

TABLE OF CONTENTS

LIST OF FIGURES

LIST OF TABLES

CHAPTER 1

INTRODUCTION

1.1 Motivation

Agriculture is the backbone of our modern society. Our stores are filled with items produced from crops grown in this country and elsewhere around the world. Needless to say, farming is important and so are the tools used in the process. Tractors are one of the necessary tools used in farming, and as technology has increased over the years, so has the level of technology in tractors. Modern tractors are starting to use GPS tracking and automated metering systems that allow farmers to be more efficient not only with the time it takes to do a job but also with wasting less product and raw material. As GPS tracking systems become more competitive and advanced, better understanding of the tractor and implement behavior is important in enabling the tracking systems to be more accurate and have better overall performance. Figure 1.1 shows an image of a field furrowed using GPS guidance.

Figure 1.1: Field Furrowed Using GPS Guidance

Gaining a better understanding of tractor and implement behavior through mathematical modeling is the motivation behind the research in this thesis. A more accurate system model naturally creates a more accurate control system that is based on that model. Figure 1.2 shows a tractor pulling a hitched cultivator.

Figure 1.2: Tractor Pulling a Cultivator

1.2 Background

Much yaw dynamic modeling of tractors has been done in the past for the purpose of tractor control. Many of the models are based on the Traditional Bicycle (TB) Model form. For example, a simplification of the TB model was used by the researchers in [1] to form a simple kinematic model. Also, Rekow [2] used assumptions to form a simpler first order model called the Neutral Steer (NS) Model. Alternately, O'Connor [3] looked at a model used by Ellis [4] that neglects lateral tire dynamics and also a similar bicycle model that uses Wong's tire model [5]; both of these models assume constant forward velocity. Owen and Bernard used a TB Model with added front and rear tire relaxation lengths for studying a tractor-loader-backhoe [6], while Bevly found that just adding front tire relaxation lengths was adequate for his modeling [7].

Additionally, tractor-implement models have been looked at by different researchers. A tractor towed-implement dynamic model was developed by Bell [8]. Bevly developed a tractor towed-implement model based on the simple kinematic model [9]. Feng developed a tractor towed-implement model by adding a towed implement model to the TB model [10]. A tractor hitched implement model developed by O'Connor used Wong's tire model to describe the hitch dynamics [3]. The O'Connor model is similar to the "3-wheeled" Bicycle Model developed in this thesis in that the hitched implement forces are generated using a tire model; however, the derivations of the two models are different. For example, the O'Connor model is a five state model, where the "3-wheeled" Bicycle Model developed in this thesis is a two state model. Bukta collected data on a tractor with and without hitched implements to determine the effects of hitch free-play on the tractor's dynamics [11].

1.3 Purpose of Thesis and Contribution

The purpose of this thesis is to derive a yaw dynamic model which can capture and quantify the effects that a hitched implement such as a ripper imposes on the tractor. Deriving such a model will provide a more accurate model which can potentially improve a controller using this model.

In this thesis, a number of both traditional and non-traditional models are derived and then compared for yaw rate tracking ability using experimental data as a basis. A model is found in which hitched implement conditions can be accounted for, and a great improvement in yaw rate tracking ability in both steady state and dynamic conditions is seen vs. traditional models.

Experiments are taken where implement forces are recorded using a hitch force dynamometer. The data are used to validate the way the hitched implement forces are derived in the new hitched implement yaw dynamic model. The experiments show that the way the implement forces are derived is reasonably correct.

Steady state and dynamic chirp data are taken for a variety of implements at varying depths and speeds. The steady state data are used to quantify the variation in the hitch parameter from implement to implement and depth to depth for the chosen hitched implement yaw dynamic model. The dynamic chirp data are used to solve for other unknown parameters of the new model. Once these parameters are known, a time and frequency analysis is done on the new hitched implement yaw dynamic model to gain understanding of its characteristics.

A model which accounts for four-wheel drive forces is also derived in this thesis. Experiments are taken which provide a preliminary look into the effect of four-wheel drive traction forces on the yaw dynamics of a tractor. A definite difference in using two-wheel drive vs. four-wheel drive is shown.

1.4 Outline of Thesis

Chapter 2 presents a general model and then derivations of several new and traditional analytical yaw dynamic models for a tractor. The models are then compared for yaw rate tracking ability, and a model which best predicts the yaw rate of a tractor with a hitched implement is chosen. Chapter 3 presents a validation of the hitched implement lateral force equation. In Chapter 4, steady state experiments are used to quantify the variations of the hitched implement parameter in the new hitched implement yaw dynamic model for various implements at varying depths. Dynamic chirp experiments are used to solve for other parameters of the new hitched implement yaw dynamic model. Chapter 5 presents a derivation of a model which accounts for the four-wheel drive traction forces present in the yaw dynamics of a four-wheel drive tractor. Experiments are used to show how much the yaw rate is actually affected in a four-wheel drive vs. non four-wheel drive setup.

CHAPTER 2

ANALYTICAL MODELING OF THE TRACTOR

2.1 Introduction

In this chapter, a variation of the bicycle model, termed the “3 wheeled” Bicycle Model is developed. This model takes into account the effects of a hitched implement. This model with added front and hitch relaxation lengths is then compared with various models used by other researchers in vehicle applications. It is shown that this model can most accurately represent the dynamics of a tractor with a hitched implement.

2.2 The General Diagram

The general diagram from which all the models in this chapter can be derived is shown in Figure 2.1. The vectors and angles in this figure show a positive sign convention, which associates positive forces with negative slip angles. The diagram represents a 4WD tractor with a hitched implement. In this general diagram, the hitched implement is modeled as two tires at the hitch designating that the left and right sides of the implement may have differing conditions. Table 2.1 describes the variables found in Figure 2.1. Equations (2.1-2.3) represent the dynamic equations of motion for the tractor, which are derived from the general diagram by summing all the forces and moments

acting on the tractor. Equation (2.2) takes into account the lateral acceleration from total vehicle sideslip through the $m \cdot V \cdot r \cdot \cos(\beta)$ term.

$$\sum F_x = F_{Trl} + F_{Trr} - F_{xhl} - F_{xhr} + F_{Tfl} \cdot \cos(\delta_l) + F_{Tfr} \cdot \cos(\delta_r) = m\ddot{x} \tag{2.1}$$

$$\sum F_y = m \cdot a_y = F_{yhl} + F_{yhr} + F_{yrl} + F_{yrr} + F_{Tfl} \cdot \sin(\delta_l) + F_{Tfr} \cdot \sin(\delta_r) + F_{yfl} \cdot \cos(\delta_l) + F_{yfr} \cdot \cos(\delta_r) = m\dot{V}_y + m \cdot V \cdot r \cdot \cos(\beta) \tag{2.2}$$

$$\sum M_{CG} = F_{Tfl} \cdot \sin(\delta_l) \cdot a + F_{Tfr} \cdot \sin(\delta_r) \cdot a + F_{yfl} \cdot \cos(\delta_l) \cdot a + F_{yfr} \cdot \cos(\delta_r) \cdot a + F_{Tfl} \cdot \cos(\delta_l) \cdot \frac{t}{2} - F_{Tfr} \cdot \cos(\delta_r) \cdot \frac{t}{2} + F_{Trl} \cdot \frac{t}{2} - F_{Trr} \cdot \frac{t}{2} - F_{yfl} \cdot \sin(\delta_l) \cdot \frac{t}{2} + F_{yfr} \cdot \sin(\delta_r) \cdot \frac{t}{2} - F_{yhl} \cdot (b+c) - F_{yhr} \cdot (b+c) - F_{yrl} \cdot b + F_{yrr} \cdot b - F_{xhl} \cdot L_1 + F_{xhr} \cdot L_1 = I_z \cdot \dot{r} \tag{2.3}$$

Where I_z is the mass moment of inertia of the tractor and implement.

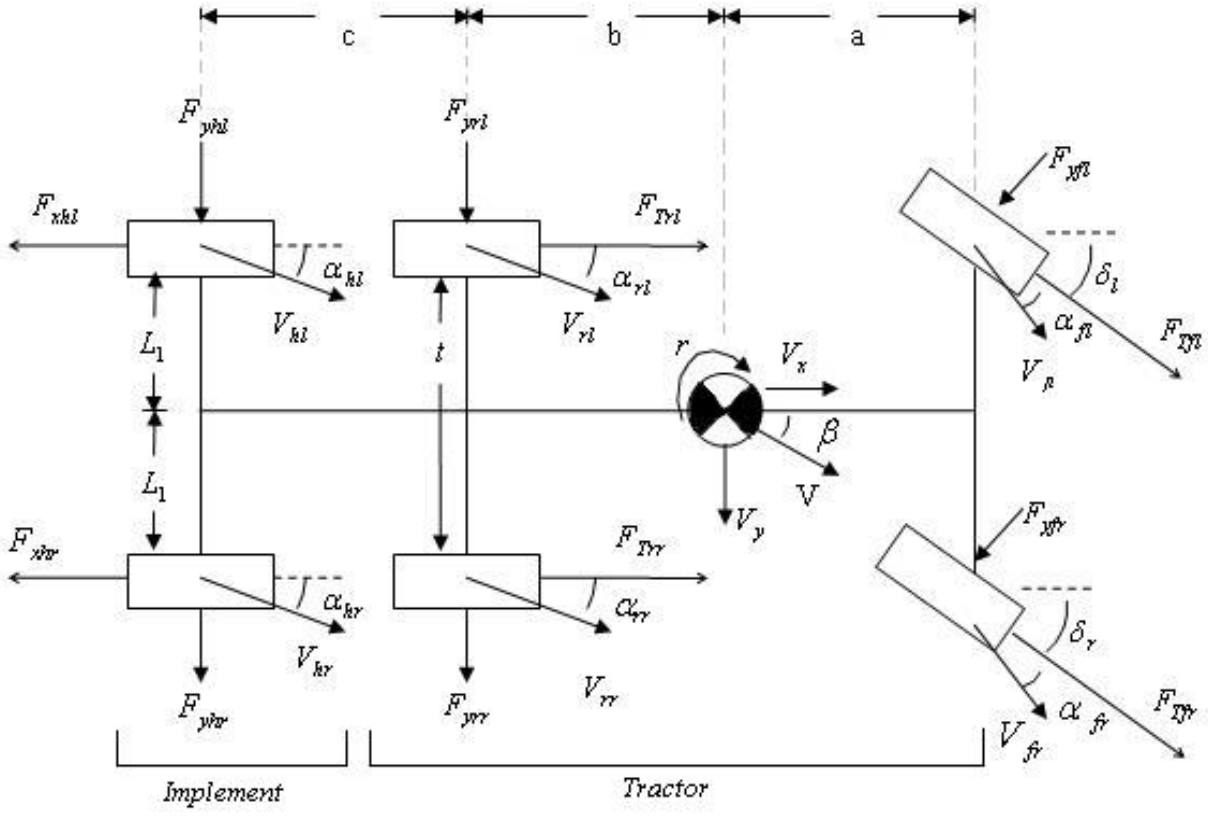

Figure 2.1: The General Diagram Depicting a 4WD Tractor with a Hitched Implement

Table 2.1: The General Diagram Parameters

$F_{yfl} \& F_{yfr}$	Front tire lateral forces for the left and right side of the vehicle, respectively
$F_{yrl} \& F_{yrr}$	Rear tire lateral forces
$F_{yhl} \& F_{yhr}$	Implement lateral forces
$F_{Tfl} \& F_{Tfr}$	Front tire traction forces
$F_{Trl} \& F_{Trr}$	Rear tire traction forces
$F_{xhl} \& F_{xhr}$	Implement draft forces
$\delta_l \& \delta_r$	Steering angles
$\alpha_{fl} \& \alpha_{fr}$	Slip angles for the front tires
$\alpha_{rl} \& \alpha_{rr}$	Slip angles for the rear tires
$\alpha_{hl} \& \alpha_{hr}$	Slip angles for the hitched implement
$V_{fl} \& V_{fr}$	Front tire velocities
$V_{rl} \& V_{rr}$	Rear tire velocities
$V_{hl} \& V_{hr}$	Hitch velocities
V	Vehicle velocity
V_x	Vehicle forward velocity
V_y	Vehicle lateral velocity
β	Vehicle sideslip angle
r	Yaw rate
a	Distance from center of front wheels to center of gravity
b	Distance from center of rear wheels to center of gravity
c	Distance from hitch to center of rear wheels
t	Track width of the tractor
L_1	Distance between centers of force action on implement

2.3 The "3 Wheeled" Bicycle Model

The "3-wheeled" Bicycle Model is developed from Figure 2.1 by making the following simplifications. It is natural to make as many simplifications as possible because this leads to a less computationally intensive and/or linear model.

The tire sideslip angle is defined as the angle between the longitudinal axis of the tire and the velocity vector at the tire. Therefore, the tire slip angles can be calculated from the longitudinal and lateral velocity at the tire as shown in Equations (2.4-2.9).

$$\alpha_{rl} = \tan^{-1}\left(\frac{V_y - b\cdot r}{V_x - \frac{1}{2}t\cdot r}\right) \tag{2.4}$$

$$\alpha_{rr} = \tan^{-1}\left(\frac{V_y - b\cdot r}{V_x + \frac{1}{2}t\cdot r}\right) \tag{2.5}$$

$$\alpha_{fl} = \tan^{-1}\left(\frac{V_y + a\cdot r}{V_x - \frac{1}{2}t\cdot r}\right) - \delta_l \tag{2.6}$$

$$\alpha_{fr} = \tan^{-1}\left(\frac{V_y + a\cdot r}{V_x + \frac{1}{2}t\cdot r}\right) - \delta_r \tag{2.7}$$

$$\alpha_{hl} = \tan^{-1}\left(\frac{V_y - (b+c)\cdot r}{V_x - \frac{1}{2}t\cdot r}\right) \tag{2.8}$$

$$\alpha_{hr} = \tan^{-1}\left(\frac{V_y - (b+c)\cdot r}{V_x + \frac{1}{2}t\cdot r}\right) \tag{2.9}$$

If $V_x >> \frac{1}{2}t\cdot r$, and assuming left and right steering angles are the same, $\delta_l = \delta_r$, then

$$\alpha_{fl} \approx \alpha_{fr} = \alpha_f = \tan^{-1}\left(\frac{V_y + a \cdot r}{V_x}\right) - \delta \tag{2.10}$$

$$\alpha_{rl} \approx \alpha_{rr} = \alpha_r = \tan^{-1}\left(\frac{V_y - b \cdot r}{V_x}\right) \tag{2.11}$$

$$\alpha_{hl} \approx \alpha_{hr} = \alpha_h = \tan^{-1}\left(\frac{V_y - (b+c) \cdot r}{V_x}\right) \tag{2.12}$$

Also, if vehicle sideslip angle, β is assumed to be small, then

$$\alpha_f = \frac{V_y + a \cdot r}{V_x} - \delta \tag{2.13}$$

$$\alpha_r = \frac{V_y - b \cdot r}{V_x} \tag{2.14}$$

$$\alpha_h = \frac{V_y - (b+c) \cdot r}{V_x} \tag{2.15}$$

Assuming the same tires are on the left and right sides and that there is no weight transfer from left to right enables

$$F_{yfl} \approx F_{yfr} = F_{yf\_tire} \tag{2.16}$$

$$F_{yrl} \approx F_{yrr} = F_{yr\_tire} \tag{2.17}$$

so that

$$F_{yf} = 2 \cdot F_{yf\_tire} \tag{2.18}$$

$$F_{yr} = 2 \cdot F_{yr\_tire} \tag{2.19}$$

The left and right tire traction forces are assumed to be the same.

$$F_{Tfl} \approx F_{Tfr} = F_{Tf\_tire} \tag{2.20}$$

$$F_{Trl} \approx F_{Trr} = F_{Tr\_tire} \tag{2.21}$$

$$F_{trac} = 2 \cdot F_{Tf\_tire} \tag{2.22}$$

$$F_{Tr} = 2 \cdot F_{Tr\_tire} \tag{2.23}$$

The left and right draft forces are also assumed to be the same.

$$F_{xhr} \approx F_{xhl} = F_{xh\_side} \tag{2.24}$$

This allows any moment from the difference in the forces, shown below in Equation (2.25), to be dropped out.

$$M_{diff} = F_{xhr} \cdot L_1 - F_{xhl} \cdot L_1 \tag{2.25}$$

Validation of this assumption is given in Chapter 3. Also, the total implement draft force becomes that defined by Equation (2.26)

$$F_{xh} = 2 \cdot F_{xh\_side} \tag{2.26}$$

The left and right implement lateral forces are also assumed to be the same, and the total lateral implement force becomes that shown in Equation (2.28)

$$F_{yhr} \approx F_{yhl} = F_{yh\_side} \tag{2.27}$$

$$F_{yh} = 2 \cdot F_{yh\_side} \tag{2.28}$$

Tractor mass and center of gravity location are assumed constant. Because M_{diff} is ignored and yaw modeling, not longitudinal modeling, is being done, the summation of forces in the longitudinal axis is not needed and is left out. If the front traction forces are not neglected, a FBD for the "3-wheeled" Bicycle Model which takes into account four-wheel drive effects can be created and is shown in Figure 2.2. This model is specifically dealt with in Chapter 5.

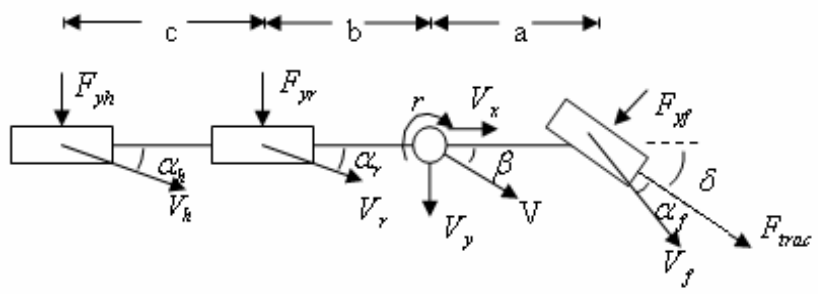

Figure 2.2: "3-wheeled" Bicycle Model Which Takes Into Account Front Traction Forces

However, neglecting the four-wheel drive (front axle) traction forces and using the other simplifications allow Figure 2.3 to be used as the FBD of the "3-wheeled" Bicycle Model.

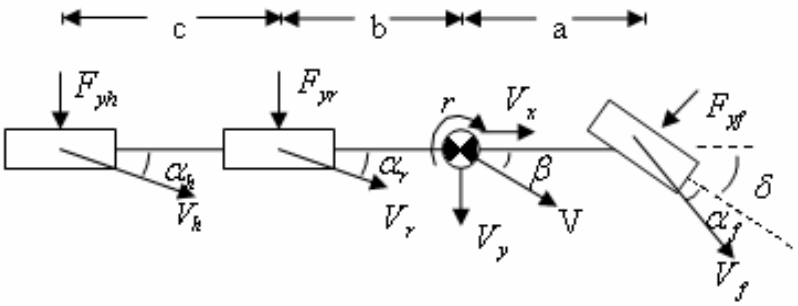

Figure 2.3: The "3-wheeled" Bicycle Model FBD

Table 2.2: The "3-wheeled" Bicycle Model Specific Parameters

α_h	Hitch side slip angle
F_{yh}	Lateral force at the hitch
$C_{\alpha h}$	Hitch cornering stiffness
α_r	Tractor rear tire side slip angle
α_f	Tractor front tire side slip angle
$C_{\alpha r}$	Tractor rear tire cornering stiffness, per axle
$C_{\alpha f}$	Tractor front tire cornering stiffness, per axle
δ	Steering angle
F_{yr}	Lateral force on the rear tractor tire
F_{yf}	Lateral force on the front tractor tire
V_r	Velocity of the rear tire
V_f	Velocity of the front tire

Summing the forces in the lateral and vertical axes of the tractor yields Equations (2.29-2.30).

$$\sum F_y = m \cdot a_y = F_{yh} + F_{yr} + F_{yf} \cdot \cos(\delta) = m\dot{V}_y + m \cdot V \cdot r \cdot \cos(\beta) \quad (2.29)$$

$$\sum M_{CG} = F_{yf} \cdot \cos(\delta) \cdot a - F_{yh} \cdot (b + c) - F_{yr} \cdot b = I_z \cdot \dot{r} \quad (2.30)$$

The small β assumption causes $\cos(\beta) \approx 1$ and assuming small steering angles allows $\cos(\delta) \approx 1$, so that Equations (2.29-2.30) become Equations (2.31-2.32).

$$m\dot{V}_y + m \cdot V \cdot r = m \cdot a_y = F_{yh} + F_{yr} + F_{yf} \tag{2.31}$$

$$I_z \cdot \dot{r} = F_{yf} \cdot a - F_{yr} \cdot b - F_{yh} \cdot (b + c) \tag{2.32}$$

Equations (2.33-2.35) represent the forces at the tires and are derived from the linear tire model given in Equation (3.3).

$$F_{yf} = -C_{\alpha f} \cdot \alpha_f \tag{2.33}$$

$$F_{yr} = -C_{\alpha r} \cdot \alpha_r \tag{2.34}$$

$$F_{yh} = -C_{\alpha h} \cdot \alpha_h \tag{2.35}$$

Where

$$C_{\alpha f} = 2 \cdot C_{\alpha f\_tire} \tag{2.36}$$

$$C_{\alpha r} = 2 \cdot C_{\alpha r\_tire} \tag{2.37}$$

Substituting Equations (2.33-2.35) into Equations (2.31-2.32) yields Equations (2.38-2.39) shown below.

$$m\dot{V}_y + m \cdot V \cdot r = -C_{\alpha h} \cdot \alpha_h - C_{\alpha r} \cdot \alpha_r - C_{\alpha f} \cdot \alpha_f \tag{2.38}$$

$$I_z \cdot \dot{r} = C_{\alpha h} \cdot \alpha_h \cdot (b + c) + C_{\alpha r} \cdot \alpha_r \cdot b - C_{\alpha f} \cdot \alpha_f \cdot a \tag{2.39}$$

Using the small β assumption to say $V_x \approx V$, substituting Equations (2.13-2.15) into Equations (2.38-2.39), and organizing the resulting equations into state space form yields the state space form of the "3-wheeled" Bicycle Model, which is given in Equation (2.40).

$$\begin{bmatrix} \dot{V}_y \\ \dot{r} \end{bmatrix} = \begin{bmatrix} \dfrac{-(C_{\alpha h} + C_{\alpha r} + C_{\alpha f})}{m \cdot V} & \dfrac{((b+c) \cdot C_{\alpha h} + b \cdot C_{\alpha r} - a \cdot C_{\alpha f})}{m \cdot V} - V \\ \dfrac{((b+c) \cdot C_{\alpha h} + b \cdot C_{\alpha r} - a \cdot C_{\alpha f})}{I_z \cdot V} & \dfrac{-((b+c)^2 \cdot C_{\alpha h} + b^2 \cdot C_{\alpha r} + a^2 \cdot C_{\alpha f})}{I_z \cdot V} \end{bmatrix} \cdot \begin{bmatrix} V_y \\ r \end{bmatrix} + \begin{bmatrix} \dfrac{C_{\alpha f}}{m} \\ \dfrac{a \cdot C_{\alpha f}}{I_z} \end{bmatrix} \cdot \delta \quad (2.40)$$

This state space model can be transformed using a Laplace transformation to yield the transfer function given in Equation (2.41). This transfer function has an input of steering angle and an output of yaw rate.

$$\frac{r(s)}{\delta(s)} = \frac{C_{\alpha f} a \cdot s + \dfrac{C_{\alpha f} \cdot C_1 + C_{\alpha f} a \cdot C_2}{mV}}{I_z \cdot s^2 + \left(\dfrac{C_2 \cdot I_z}{mV} + \dfrac{C_3}{V} \right) s + \left[\dfrac{C_2 \cdot C_3 - (C_1)^2}{mV^2} + C_1 \right]} \quad (2.41)$$

Where

$$C_1 = ((b+c) \cdot C_{\alpha h} + b \cdot C_{\alpha r} - a \cdot C_{\alpha f})$$

$$C_2 = (C_{\alpha h} + C_{\alpha r} + C_{\alpha f}) \quad (2.42)$$

$$C_3 = ((b+c)^2 C_{\alpha h} + C_{\alpha r} b^2 + C_{\alpha f} a^2)$$

2.4 Other Bicycle Models

This section lists alternative models used in vehicle dynamics. These other models have been developed so that the "3-wheeled" Bicycle Model can be compared to models used in previous research.

2.4.1 The Traditional Bicycle Model

The Traditional Bicycle Model is a more rudimentary form of the "3-wheeled" Bicycle Model [12]. It can be also viewed in the sense that the "3-wheeled" Bicycle Model is a more complicated version of the Traditional Bicycle Model. Both models are

derived in the same manner from Figure 2.1 except that the Bicycle Model neglects implement effects in any axis. Figure 2.4 is the free body diagram for the Traditional Bicycle Model. Equation (2.43) is the resulting state space form for this model.

$$\begin{bmatrix} \dot{V}_y \\ \dot{r} \end{bmatrix} = \begin{bmatrix} \dfrac{-(C_{ar}+C_{af})}{m\cdot V} & \dfrac{(b\cdot C_{ar}-a\cdot C_{af})}{m\cdot V} - V \\ \dfrac{(b\cdot C_{ar}-a\cdot C_{af})}{I_z\cdot V} & \dfrac{-(b^2\cdot C_{ar}+a^2\cdot C_{af})}{I_z\cdot V} \end{bmatrix} \cdot \begin{bmatrix} V_y \\ r \end{bmatrix} + \begin{bmatrix} \dfrac{C_{af}}{m} \\ \dfrac{a\cdot C_{af}}{I_z} \end{bmatrix} \delta \tag{2.43}$$

Likewise, Equation (2.44) is the transfer function form of Equation (2.43) derived from a Laplace transformation.

$$\frac{r(s)}{\delta(s)} = \frac{C_{\alpha f}\, a\cdot s + \dfrac{C_{\alpha f}\cdot C_1 + C_{\alpha f}\, a\cdot C_2}{mV}}{I_z\cdot s^2 + \left(\dfrac{C_2\cdot I_z}{mV} + \dfrac{C_3}{V}\right)s + \left[\dfrac{C_2\cdot C_3 - (C_1)^2}{mV^2} + C_1\right]} \tag{2.44}$$

Where

$$\begin{aligned} C_1 &= (b\cdot C_{ar} - a\cdot C_{af}) \\ C_2 &= (C_{ar} + C_{af}) \\ C_3 &= (C_{\alpha r} b^2 + C_{\alpha f} a^2) \end{aligned} \tag{2.45}$$

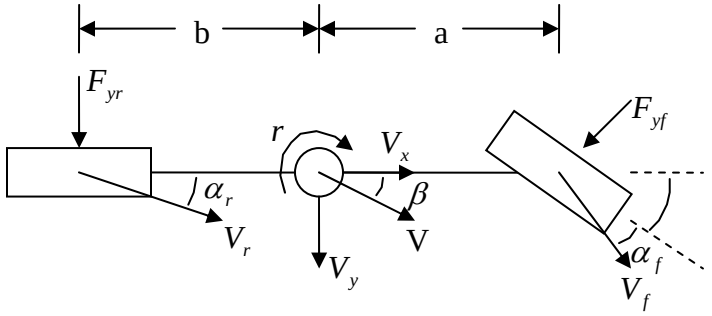

Figure 2.4: The Traditional Bicycle Model

2.4.2 Neutral Steer Bicycle Model

The Neutral Steer Bicycle Model is a special case of the Traditional Bicycle Model where the understeer gradient is equal to zero [2]. A neutral steer vehicle is defined as a vehicle whose ratio of the weight on the front wheels divided by the cornering stiffness of the front tire is equal to the ratio of the weight on the rear wheels divided by the cornering stiffness of the rear tire. A oversteer vehicle tends to spin out in cornering while an understeer vehicle tends to plow in cornering and a neutral steer vehicle does neither. The understeer gradient is defined in Equation (2.46).

$$k_{us} = \frac{W_f}{C_{\alpha f}} - \frac{W_r}{C_{\alpha r}} \tag{2.46}$$

where W_f and W_r are the weights at the front and rear axles, respectively. Setting the understeer gradient to zero yields

$$\frac{W_f}{C_{\alpha f}} = \frac{W_r}{C_{\alpha r}} \tag{2.47}$$

W_f and W_r in Equation (2.47) can be substituted to get

$$\frac{m \cdot g \cdot b}{C_{\alpha f}} = \frac{m \cdot g \cdot a}{C_{\alpha r}} \tag{2.48}$$

This in turn yields

$$a \cdot C_{af} - b \cdot C_{ar} = 0 \tag{2.49}$$

Substituting Equation (2.49) into Equation (2.43) allows simplifications to be made and gives the transfer function form of the Neutral Steer Bicycle Model, shown below.

$$\frac{r(s)}{\delta(s)} = \frac{\frac{C_{\alpha f} a}{I_z}}{s + \frac{C_{\alpha r} b^2 + C_{\alpha f} a^2}{I_z V}} \tag{2.50}$$

As can be seen, this model is a first order model and is simpler that the Traditional Bicycle Model, given the simulated vehicle is approximately neutral steer.

2.4.3 Kinematic Model

The Kinematic Model is also a special case of the Traditional Bicycle Model as it neglects vehicle and wheel sideslip and assumes a constant forward velocity. It provides a purely kinematic relationship from steering angle to yaw rate by assuming that the yaw rate is directly proportional to the steering angle for a slow moving vehicle [1]. Equation (2.51) represents the transfer function form of the Kinematic Model.

$$\frac{r(s)}{\delta(s)} = \frac{V}{L} \tag{2.51}$$

Where $L = a + b$, the wheelbase length.

2.4.4 Front Tire Relaxation Length Model

The Front Tire Relaxation Length (FRL) model is a more complicated version of the Traditional Bicycle Model. As the name denotes, this model has front tire relaxation lengths added to the bicycle model. The tire relaxation length, σ , is the amount a tire must roll in order to generate the steady state slip angle, α_0, at the tire [7].

The equation describing the tire relaxation length is a first order model and is shown in Equation (2.52).

$$\dot{\alpha}_f = \frac{V_x}{\sigma_f} \cdot \left(\alpha_{fo} - \alpha_f \right) \tag{2.52}$$

Where σ_f is the front tire relaxation length. Incorporating this equation into the equations of motion for the bicycle model and arranging them into the state space form of the front tire relaxation length model yields Equation (2.53).

$$\begin{bmatrix} \dot{V}_y \\ \dot{r} \\ \dot{\alpha}_f \end{bmatrix} = \begin{bmatrix} \frac{-C_{ar}}{m \cdot V} & \frac{b \cdot C_{ar}}{m \cdot V} - V & \frac{-C_{af}}{m} \\ \frac{b \cdot C_{ar}}{I_z \cdot V} & \frac{-b^2 \cdot C_{ar}}{I_z \cdot V} & \frac{-a \cdot C_{af}}{I_z} \\ \frac{1}{\sigma_f} & \frac{a}{\sigma_f} & \frac{-V}{\sigma_f} \end{bmatrix} \cdot \begin{bmatrix} V_y \\ r \\ \alpha_f \end{bmatrix} + \begin{bmatrix} 0 \\ 0 \\ \frac{-V}{\sigma_f} \end{bmatrix} \cdot \delta \tag{2.53}$$

The first use of this particular model was seen by Bevly in [9]. He showed that only a front tire relaxation length was adequate for his modeling, whereas the authors in [6] used a model with front and rear relaxation lengths. Bevly also showed that the Front Tire Relaxation Length Model was necessary to adequately describe the tractor's handling dynamics where a Traditional Bicycle Model was not adequate.

2.4.5 "3 Wheeled" Front Tire Relaxation Length Model

The "3 Wheeled" Front Tire Relaxation Length Model ("3-wheeled" FRL Model) is similar to the FRL Model in that a front tire relaxation length is added to the "3-wheeled" Bicycle Model instead of the Traditional Bicycle Model. The equations of motion for the "3-wheeled" Front Tire Relaxation Length Model placed in state space form are shown in Equation (2.54).

$$\begin{bmatrix} \dot{V}_y \\ \dot{r} \\ \dot{\alpha}_f \end{bmatrix} = \begin{bmatrix} \frac{-(C_{\alpha h}+C_{\alpha r})}{m\cdot V} & \frac{((b+c)\cdot C_{\alpha h}+b\cdot C_{\alpha r})}{m\cdot V}-V & \frac{-C_{\alpha f}}{m} \\ \frac{((b+c)\cdot C_{\alpha h}+b\cdot C_{\alpha r})}{I_z\cdot V} & \frac{-((b+c)^2\cdot C_{\alpha h}+b^2\cdot C_{\alpha r})}{I_z\cdot V} & \frac{-a\cdot C_{\alpha f}}{I_z} \\ \frac{1}{\sigma_f} & \frac{a}{\sigma_f} & \frac{-V}{\sigma_f} \end{bmatrix} \cdot \begin{bmatrix} V_y \\ r \\ \alpha_f \end{bmatrix} + \begin{bmatrix} 0 \\ 0 \\ \frac{-V}{\sigma_f} \end{bmatrix} \cdot \delta \qquad (2.54)$$

2.4.6 "3 Wheeled" Front and Rear Tire Relaxation Length Model

The model shown below in Equation (2.55) is the "3-wheeled" Bicycle Model with added front and rear tire relaxation lengths ("3-wheeled" FRRL Model). This model and the next model derived are for investigating if only a front tire relaxation length is adequate as shown by [9]. However, it may be the case where front relaxation lengths are not adequate to describe the dynamics, but a model with front plus rear or hitch relaxations is adequate. The equation describing the rear tire relaxation length is shown below.

$$\dot{\alpha}_r = \frac{V_x}{\sigma_r}\cdot(\alpha_{ro}-\alpha_r) \qquad (2.55)$$

Where σ_r is the rear tire relaxation length. Both Equation (2.52) and Equation (2.55) are incorporated into Equations (2.38-39) to develop the state space model for the "3-wheeled" FRRL Model shown in Equation (2.56).

$$\begin{bmatrix} \dot{V}_y \\ \dot{r} \\ \dot{\alpha}_f \\ \dot{\alpha}_r \end{bmatrix} = \begin{bmatrix} \frac{-(C_{ah})}{m\cdot V} & \frac{((b+c)\cdot C_{ah})}{m\cdot V}-V & \frac{-C_{af}}{m} & \frac{-C_{ar}}{m} \\ \frac{((b+c)\cdot C_{ah})}{I_z\cdot V} & \frac{-((b+c)^2\cdot C_{ah})}{I_z\cdot V} & \frac{-a\cdot C_{af}}{I_z} & \frac{b\cdot C_{ar}}{I_z} \\ \frac{1}{\sigma_f} & \frac{a}{\sigma_f} & \frac{-V}{\sigma_f} & 0 \\ \frac{1}{\sigma_r} & \frac{-b}{\sigma_r} & 0 & \frac{-V}{\sigma_r} \end{bmatrix} \cdot \begin{bmatrix} V_y \\ r \\ \alpha_f \\ \alpha_r \end{bmatrix} + \begin{bmatrix} 0 \\ 0 \\ \frac{-V}{\sigma_f} \\ 0 \end{bmatrix} \cdot \delta \qquad (2.56)$$

2.4.7 "3 Wheeled" Front, Rear, and Hitch Relaxation Length Model

The "3-wheeled" Bicycle Model with added front and rear tire and hitch relaxation lengths ("3-wheeled" FRHRL Model) is similar to the "3-wheeled" FRRL Model except hitch relaxation lengths are also added. The equation describing the hitch relaxation length, σ_h, is shown below.

$$\dot{\alpha}_h = \frac{V_x}{\sigma_h} \cdot (\alpha_{ho} - \alpha_h) \tag{2.57}$$

Equation (2.52), Equation (2.55), and Equation (2.57) are incorporated with the "3-wheeled" Bicycle Model's equations, and arranging in state space yields the state space form of the "3-wheeled" FRHRL Model, shown in Equation (2.58) below.

$$\begin{bmatrix} \dot{V}_y \\ \dot{r} \\ \dot{\alpha}_f \\ \dot{\alpha}_r \\ \dot{\alpha}_h \end{bmatrix} = \begin{bmatrix} 0 & -V & \frac{-C_{af}}{m} & \frac{-C_{ar}}{m} & \frac{-C_{ah}}{m} \\ 0 & 0 & \frac{-a \cdot C_{af}}{I_z} & \frac{b \cdot C_{ar}}{I_z} & \frac{(b+c) \cdot C_{ah}}{I_z} \\ \frac{1}{\sigma_f} & \frac{a}{\sigma_f} & \frac{-V}{\sigma_f} & 0 & 0 \\ \frac{1}{\sigma_r} & \frac{-b}{\sigma_r} & 0 & \frac{-V}{\sigma_r} & 0 \\ \frac{1}{\sigma_h} & \frac{-(b+c)}{\sigma_h} & 0 & 0 & \frac{-V}{\sigma_h} \end{bmatrix} \cdot \begin{bmatrix} V_y \\ r \\ \alpha_f \\ \alpha_r \\ \alpha_h \end{bmatrix} + \begin{bmatrix} 0 \\ 0 \\ \frac{-V}{\sigma_f} \\ 0 \\ 0 \end{bmatrix} \cdot \delta \tag{2.58}$$

2.4.8 "3 Wheeled" Front and Hitch Relaxation Length Model

The "3-wheeled" Bicycle Model with added front and hitch relaxations is similar to the "3-wheeled" FRHRL Model except the rear relaxation lengths are left out. Integrating the respective relaxation lengths with Equations (2.38-39) of the "3-wheeled" Bicycle Model yields Equation (2.59).

$$\begin{bmatrix} \dot{V}_y \\ \dot{r} \\ \dot{\alpha}_f \\ \dot{\alpha}_h \end{bmatrix} = \begin{bmatrix} \frac{-(C_{ar})}{m \cdot V} & \frac{(C_{ar} \cdot b)}{m \cdot V} - V & \frac{-C_{af}}{m} & \frac{-C_{ah}}{m} \\ \frac{(C_{ar} \cdot b)}{I_z \cdot V} & \frac{-(C_{ar} \cdot b^2)}{I_z \cdot V} & \frac{-a \cdot C_{af}}{I_z} & \frac{C_{ah} \cdot (b+c)}{I_z} \\ \frac{1}{\sigma_f} & \frac{a}{\sigma_f} & \frac{-V}{\sigma_f} & 0 \\ \frac{1}{\sigma_h} & \frac{-(b+c)}{\sigma_h} & 0 & \frac{-V}{\sigma_h} \end{bmatrix} \cdot \begin{bmatrix} V_y \\ r \\ \alpha_f \\ \alpha_h \end{bmatrix} + \begin{bmatrix} 0 \\ 0 \\ \frac{-V}{\sigma_f} \\ 0 \end{bmatrix} \cdot \delta \qquad (2.59)$$

2.5 Model Comparisons

All of the models in the previous section are compared against yaw rate data taken on a Deere 8420 with single rear wheels and a four shank ripper rigidly hitched to the rear. A full description of the tractor, sensors, and data acquisition system is given in Appendix A. Appendix B gives the model parameter values used in the simulation of these models. The steering angle profile for the yaw rate data is illustrated in Figure 2.5 and shows that the steering maneuver creates a series of steady state yaw rate steps. The speed for this maneuver was four miles per hour. It should be noted that during a steady state maneuver, relaxation length terms drop out, the FRL Model breaks down into the Traditional Bicycle Model, and the "3-wheeled" FRL, FRRL, FRHRL, and FHRL Models break down into the "3-wheeled" Bicycle Model. Therefore, the FRL and the "3-wheeled" FRL, FRRL, FRHRL, and FHRL Models are left out of this particular comparison. Figures 2.6-2.8 show the tracking response of the remaining models at depths of 18, 12, and 8 inches, respectively. As can be seen, the "3-wheeled" Bicycle Model has the best yaw rate tracking response. This visual inspection is also backed by the fact that the "3-wheeled" Bicycle Model has the lowest RMS errors at each depth, shown in Table 2.3 [13]. Note that with decreasing depth, the errors of the Traditional,

Neutral Steer, and Kinematic Bicycle Models decrease. Following this trend, a property of the "3-wheeled" Bicycle Model is that it collapses to the Traditional Bicycle Model in the event that there is no implement, which is the case where the hitch cornering stiffness is zero.

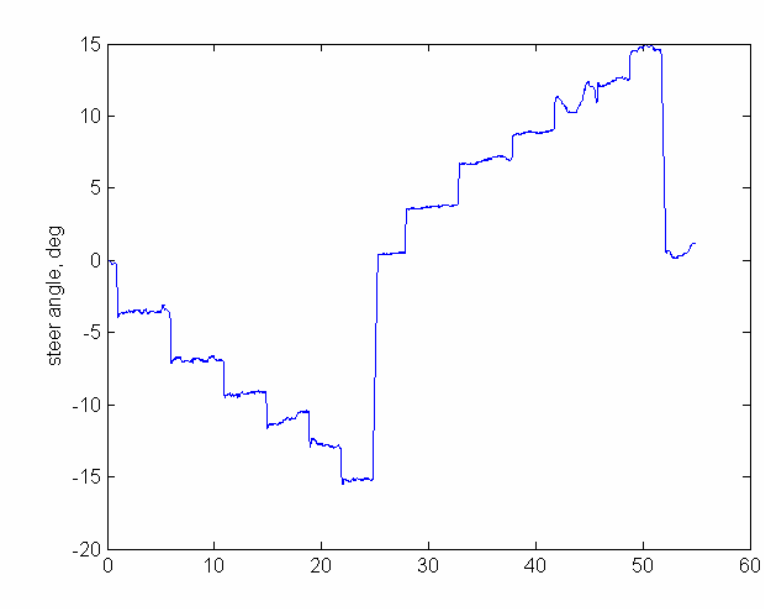

Figure 2.5: Steering Angle Profile for Figure 2.6

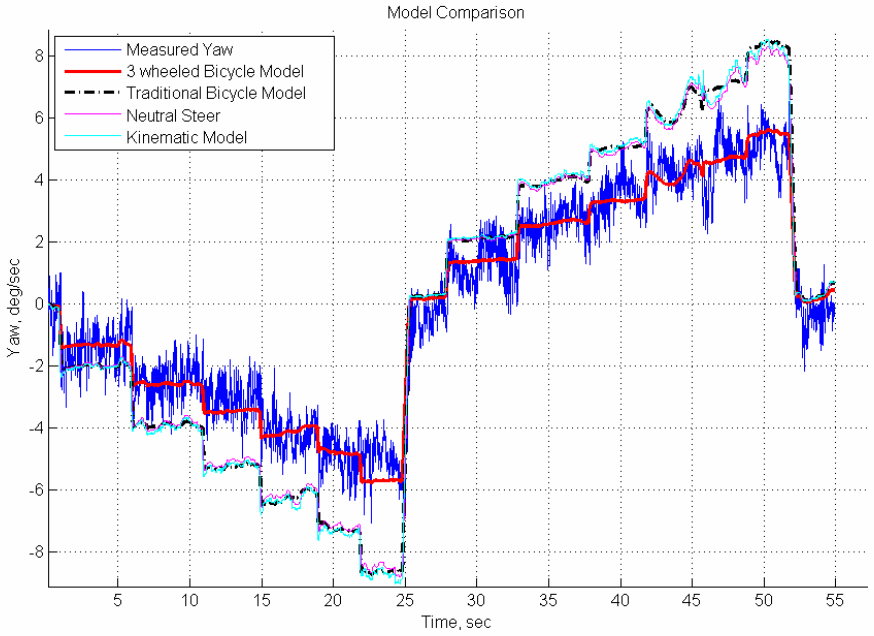

Figure 2.6: Yaw Rate Comparisons, 18 Inches Deep, 4 mph

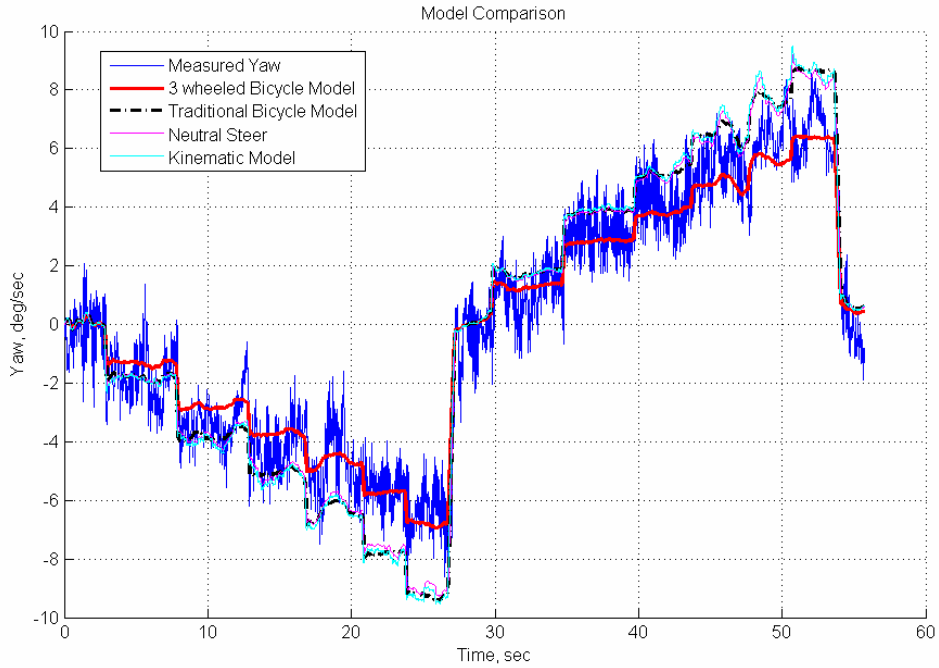

Figure 2.7: Yaw Rate Comparisons, 12 Inches Deep, 4 mph

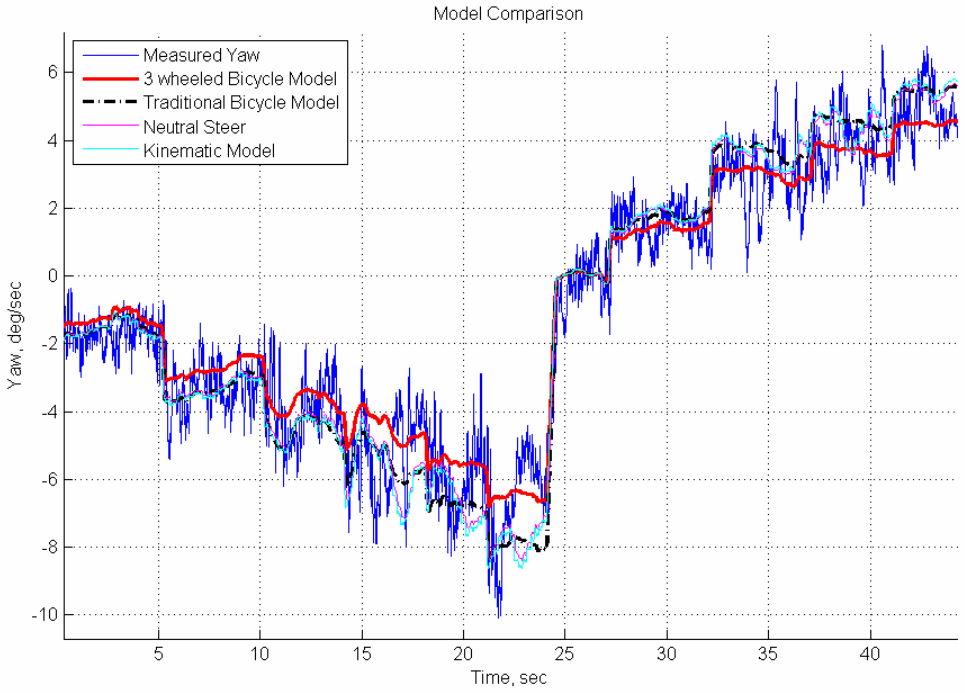

Figure 2.8: Yaw Rate Comparisons, 8 Inches Deep, 4 mph

Table 2.3: RMS Errors (deg/s) of Models at Different Depths, Static

Depth	18”	12”	8”
“3-wheeled” Bicycle Model	.24499	.4515	.49637
Traditional Bicycle Model	1.9634	1.1505	.52977
Neutral Steer Bicycle Model	1.8116	1.0508	.55075
Kinematic Model	2.0736	1.2389	.6319

Since the Kinematic, Traditional, and Neutral Steer Bicycle and FRL Models do not have adequate steady state tracking response while using an implement at depth, they are thrown out of the study at this point. It is repeated that the focus of this research is to capture and study the hitched loading effects with a given model.

The models left to study are the “3-wheeled” Bicycle Model, the “3-wheeled” FRL Model, the “3-wheeled” FRRL Model, the “3-wheeled” FHRL Model, and the “3-wheeled” FRHRL Model. These models can be differentiated with a dynamic steering maneuver. The dynamic steering maneuver chosen for this comparison is a chirp steering input shown in Figure 2.9. This maneuver also uses a four shank ripper at a depth of 18 inches at a speed of four miles per hour.

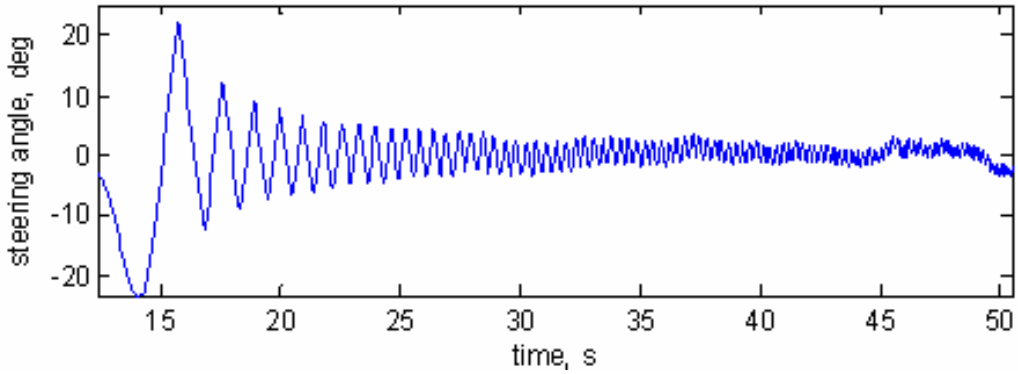

Figure 2.9: Dynamic Steering Maneuver

As a single figure would have too many models to compare at once, the comparison is broken down over several plots, Figures 2.10-2.12. Figure 2.10 is a comparison of the “3-wheeled” FRL Model and the “3-wheeled” FRRL Model. As shown by Bevly in [9], the two models have approximately the same response; therefore, the “3-wheeled” FRRL Model is thrown out of the study at this point since it is the more complex of the two. Figure 2.11 is a comparison of the “3-wheeled” FHRL Model and the “3-wheeled” FRHRL Model. Similar to the FRL and FRRL Models of Figure 2.10, these two models have approximately the same response, so the “3-wheeled” FRHRL Model is also thrown out of the study at this point. Figure 2.12 is a comparison of the

"3-wheeled" Bicycle Model, the "3-wheeled" FRL Model, and the "3-wheeled" FHRL Model. As can be seen, the model that includes hitch relaxation lengths has the best response, especially in the higher frequencies. This visual inspection is also backed by the "3-wheeled" FHRL Model having the lowest RMS error, given in Table 2.4.

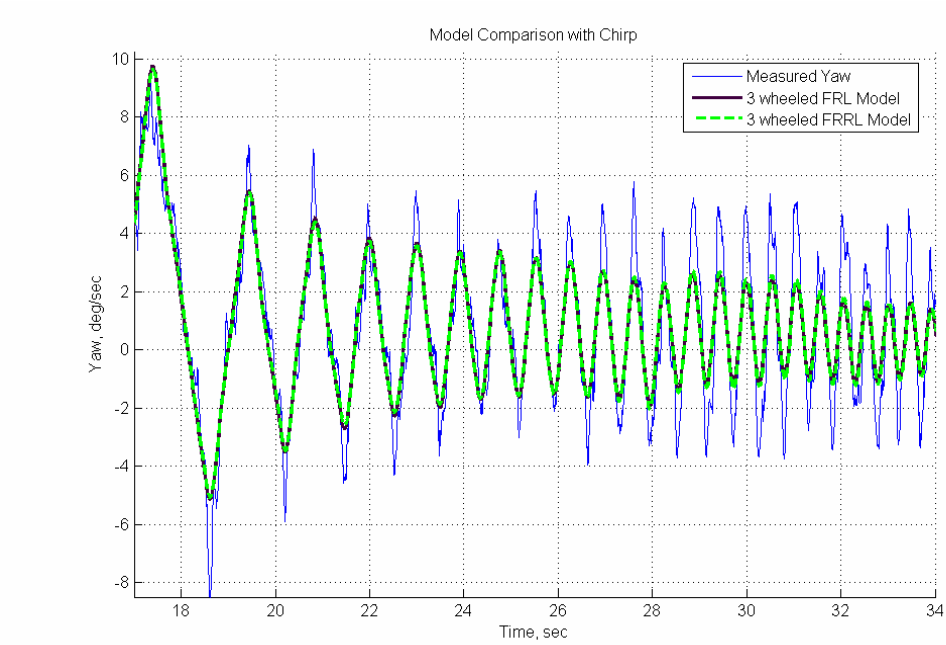

Figure 2.10: Yaw Rate Comparisons, Chirp 18 Inches Deep

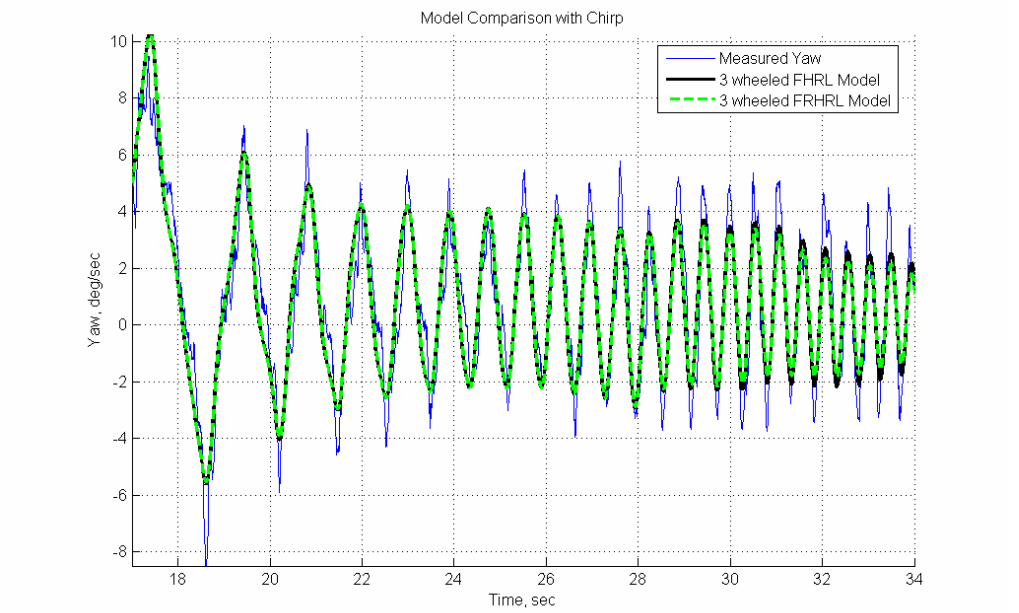

Figure 2.11: Yaw Rate Comparisons, Chirp 18 Inches Deep

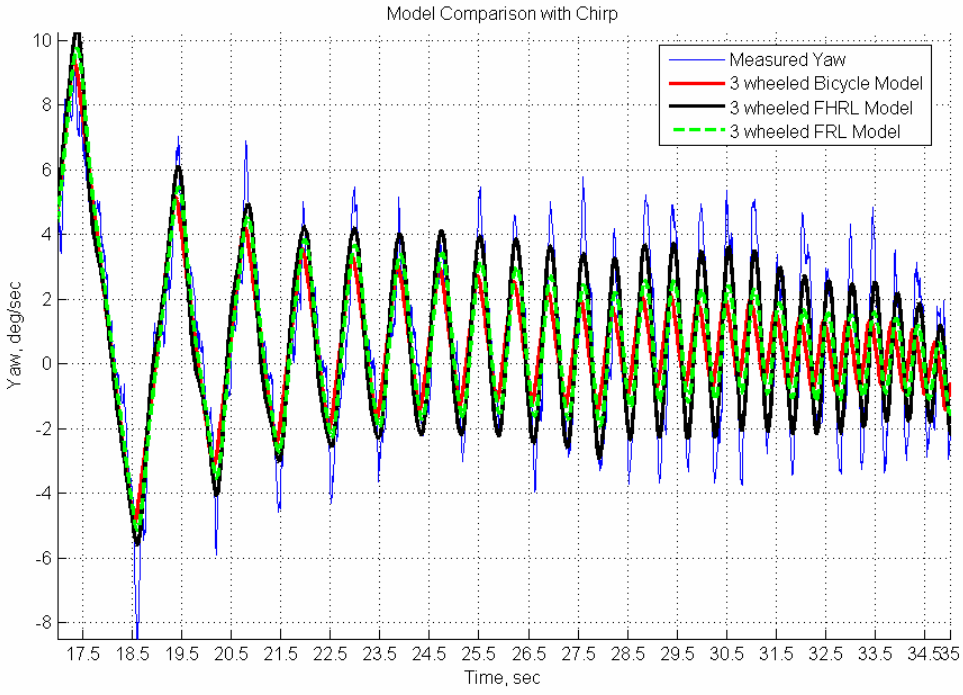

Figure 2.12: Yaw Rate Comparisons, Chirp 18 Inches Deep

Table 2.4: RMS Errors (deg/s) of Models, Dynamic Response

“3-wheeled” FHRL Model	.67457
“3-wheeled” FRL Model	.74815
“3-wheeled” Bicycle Model	1.3691

2.6 Conclusions

A number of different analytical mathematical models have been derived to show their state-space form. All of these models are based on a general diagram, and making different assumptions leads to each particular model. The “3-wheeled” Bicycle Model format is a unique derivation that is basically a bicycle model that includes hitched implement effects. A number of models can be derived by adding front tire, rear tire, or hitch relaxation lengths to the Bicycle Model or the “3-wheeled” Bicycle Model.

Based on steady state responses, the Traditional Bicycle, Neutral Steer Bicycle, Kinematic, and FRL Models are shown to have inadequate yaw rate tracking ability and therefore are not considered further for the purposes of this research. The “3-wheeled” Bicycle, “3-wheeled” FRL, “3-wheeled” FRRL, “3-wheeled” FRHRL, and “3-wheeled” FHRL Models have been shown to have excellent yaw rate tracking in steady state.

Based on dynamic responses, the “3-wheeled” FRL and “3-wheeled” FRRL Models have approximately the same response, similar to that shown by [9]. Also, the “3-wheeled” FRHRL and “3-wheeled” FHRL Models have approximately the same response. Therefore, the “3-wheeled” FRL and “3-wheeled” FHRL Models are chosen over the “3-wheeled” FRRL and “3-wheeled” FRHRL Models, respectively.

Finally, the “3-wheeled” Bicycle, “3-wheeled” FRL, and “3-wheeled” FHRL Models are compared against each other with the same dynamic steering maneuver, and it is shown that the “3-wheeled” FHRL Model provides the best static and dynamic yaw rate tracking response.

CHAPTER 3

HITCH MODELING

3.1 Introduction

This chapter validates the assumption of the implement forces being able to be modeled by the linear tire model. The validation is accomplished through taking force data from a hitch force dynomometer provided by the USDA-ARS Soil Dynamics Laboratory and comparing it to the sideslip of the implement to verify that the relationship between the two is as assumed. This chapter also shows that neglecting M_{diff}, as done by the "3-wheeled" Bicycle Model derivation, is a valid assumption.

3.2 Hitch Modeling

The following figure is a graphical representation of how a tire compares to an implement at the hitch.

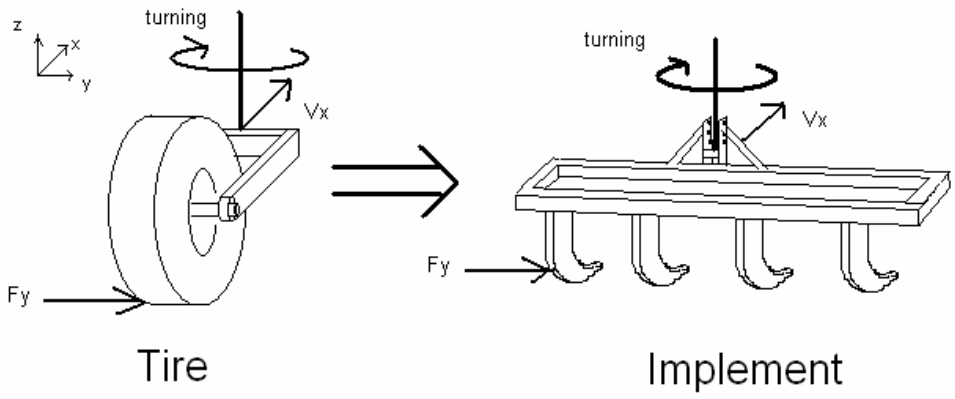

Figure 3.1: How the Tire Model Relates to an Implement

According to the linear tire model given in Equation (3.1), a force affecting the yaw dynamics of a vehicle is present only when the tire is experiencing a slip angle [12].

$$F_y = -C_\alpha \cdot \alpha \tag{3.1}$$

Slip angle is defined as the angle between the lateral and longitudinal velocities of the body in motion, shown in Equation (3.2).

$$\alpha_{body} = \tan^{-1}\left(\frac{V_{ybody}}{V_{xbody}}\right) \tag{3.2}$$

Figure 3.2 below shows a schematic of a tire with the associated lateral force. As can be seen, a deformation of the contact patch causes a slip angle, α, and a lateral force, F_y. The F_y and α of Figure 3.2 are governed by the tire curve shown in Figure 3.3. F_y peaks and becomes non-linear when it reaches a certain slip angle. This peak is determined by ground conditions. Also, within small α, the F_y is linear with the slope of the line defined by C_α. C_α is dependent on tire characteristics such as tread, wall stiffness, tire pressure, etc.

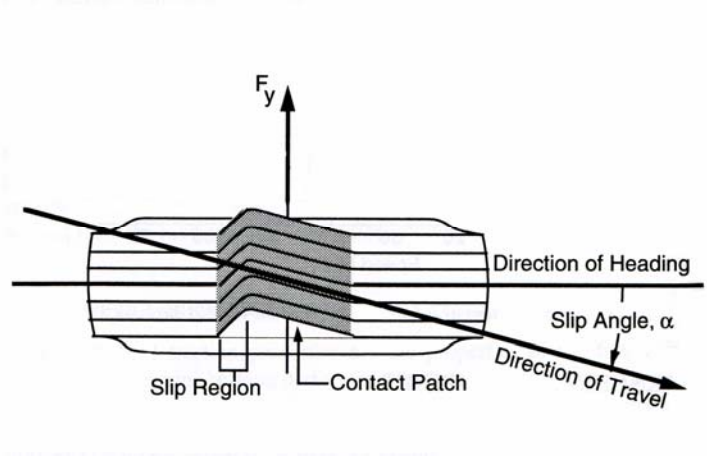

Figure 3.2: Tire Schematic, courtesy of Gillespie [12]

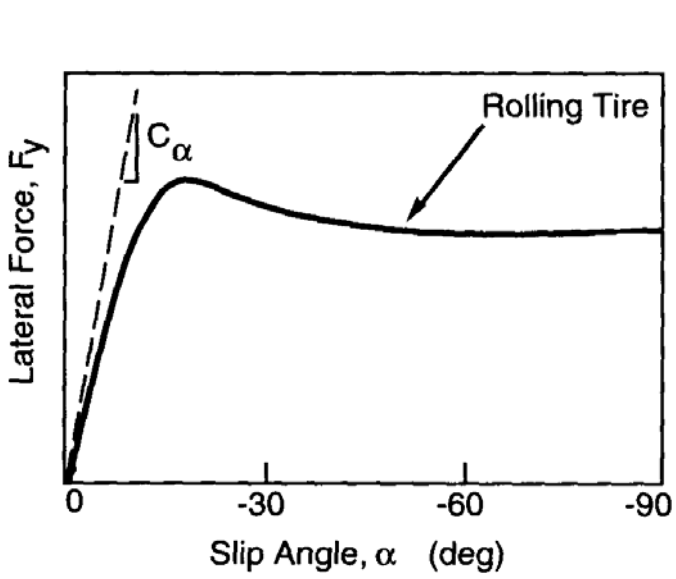

Figure 3.3: Tire Curve, courtesy of Gillespie [12]

Likewise, the "3-wheeled" Bicycle Model assumes that with an implement, in the same manner as a tire, the lateral force is proportional to the slip angle of the implement so that Equation (3.1) becomes Equation (3.3).

$$F_{yh} = -C_{\alpha h} \cdot \alpha_h \tag{3.3}$$

Section 3.4 shows that this relationship holds and the assumption is valid. Additionally, the longitudinal forces on the implement are assumed to be proportional to the implement's longitudinal velocity.

Figure 3.4 shows the schematic used to analyze the implement forces. Recall from Chapter 2 that the implement left and right lateral forces and slip angles are lumped together. This schematic demonstrates how the forces generated on the hitched implement affect the center of gravity of the tractor. Figure 3.4 does not assume that the left and right draft forces are the same. It should be noted, that for the "3-wheeled" Bicycle Model in Chapter 2, left and right draft forces are assumed to be the same, and therefore, $M_{diff} = 0$, an assumption validated in Section 3.5.

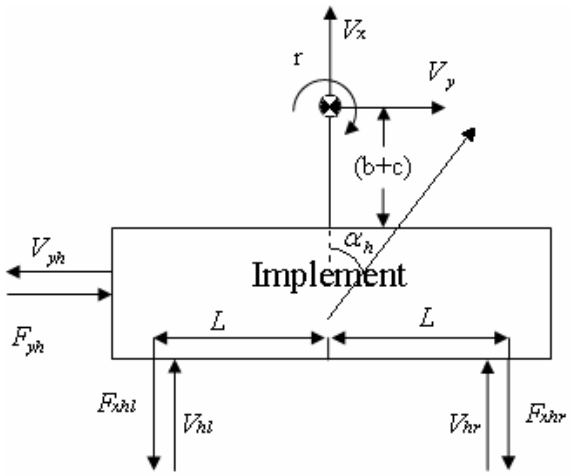

Figure 3.4: The Hitched Implement Schematic

The FBD in Figure 3.4 is used to analyze the effect that the implement's forces and moments have on the equations of motion when forming the "3-wheeled" Bicycle

Model. Summing the moments of the implement about the center of gravity of the tractor results in Equation (3.4), below.

$$M_{CGimplement} = F_{yh} \cdot (b + c) + F_{xhr} \cdot L - F_{xhl} \cdot L \tag{3.4}$$

Where:

$$F_{yh} = -C_{\alpha h} \cdot \alpha_h \tag{3.5}$$

$$F_{xhr} = C_x \cdot V_{hr} \tag{3.6}$$

$$F_{xhl} = C_x \cdot V_{hl} \tag{3.7}$$

Note that C_x is a draft coefficient and is assumed to be equal for both sides.

Substituting Equations (3.5-3.7) into Equation (3.4) yields:

$$M_{CGimplement} = -C_{\alpha h} \cdot \alpha_h \cdot (b + c) + C_x \cdot V_{hr} \cdot L - C_x \cdot V_{hl} \cdot L \tag{3.8}$$

Where:

$$V_{hr} = V_x - r \cdot L \tag{3.9}$$

$$V_{hl} = V_x + r \cdot L \tag{3.10}$$

Substituting Equations (3.9-3.10) into Equation (3.8) yields:

$$\begin{aligned} M_{CGimplement} &= -C_{\alpha h} \cdot \alpha_h \cdot (b + c) + C_x \cdot L \cdot [(V_x - r \cdot L) - (V_x + r \cdot L)] \\ &= -C_{\alpha h} \cdot \alpha_h \cdot (b + c) - 2C_x \cdot r \cdot L^2 \end{aligned} \tag{3.11}$$

The term $M_{diff} = -2C_x \cdot r \cdot L^2$ from Equation (3.11) represents the moment caused by the difference between the left and right longitudinal forces, F_{xhl} and F_{xhr}. There will always be a longitudinal draft force, F_{xh}, as long as the implement is in the

ground. However, if the left and right draft forces are not significantly different, they will not affect the tractor's yaw dynamics.

Equations (3.12-3.13) summarize the effect of the implement forces on the tractor if M_{diff} is ignored and F_{yh} can be modeled as a tire.

$$F_{yh} = -C_{\alpha h} \cdot \alpha_h \tag{3.12}$$

$$M_{CGimplement} = -C_{\alpha h} \cdot \alpha_h \cdot (b + c) \tag{3.13}$$

3.3 Data Collection

Figures 3.5 and 3.6 show the steering profile and test trajectory for the data collection experiments used to validate the implement model. The experiments are designed such that distinct lateral forces can be recorded for distinct implement slip angles. In order to validate Equation (3.12), the lateral forces and also the slip angles must be recorded so that the relationship between the two can be determined. It should be noted here that α_h was calculated from the recorded yaw rate based on the kinematics of the tractor. The equation used to calculate α_h is shown in Equation (3.14) below.

$$\alpha_h = \tan^{-1}\left(\frac{r \cdot (b + c) - V_x \cdot \sin(\beta)}{V_x}\right) \tag{3.14}$$

Where $r \cdot (b + c) - V_x \cdot \sin(\beta)$ is the lateral velocity at the hitch, V_y with $V_x \cdot \sin(\beta)$ being subtracted out as the lateral velocity caused by the total sideslip of the vehicle. The β was calculated by subtracting the GPS course measurement from the heading by integrating the yaw rate measurement shown in Equation (3.15) below.

$$\beta = v_{GPS} - \int r \tag{3.15}$$

The experiments are taken at varying depths for the purpose of defining the different implement cornering stiffnesses, $C_{\alpha h}$, and are limited to one speed due to data collection time constraints. Data was collected at 4 mph at depths of 6", 12", and 18" on a Deere 955 four-shank ripper. Multiple data runs were collected at each depth with the ripper. Appendix A details the experimental setup for these data collection runs.

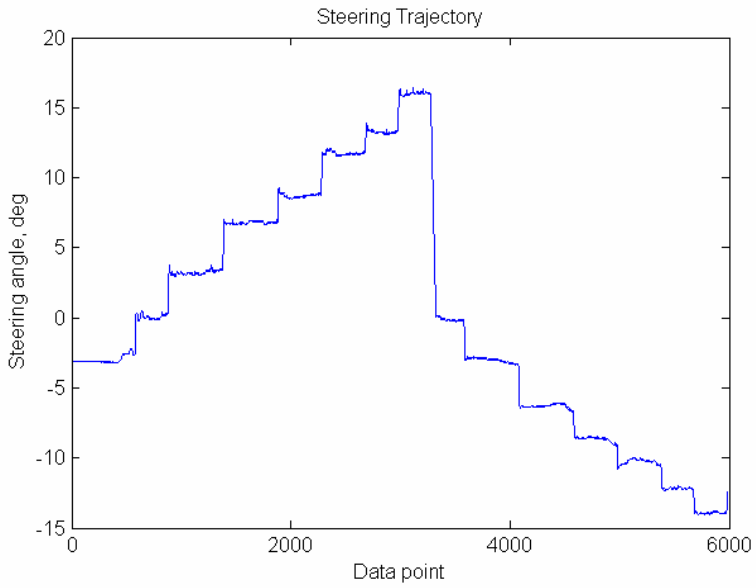

Figure 3.5: Steering Trajectory

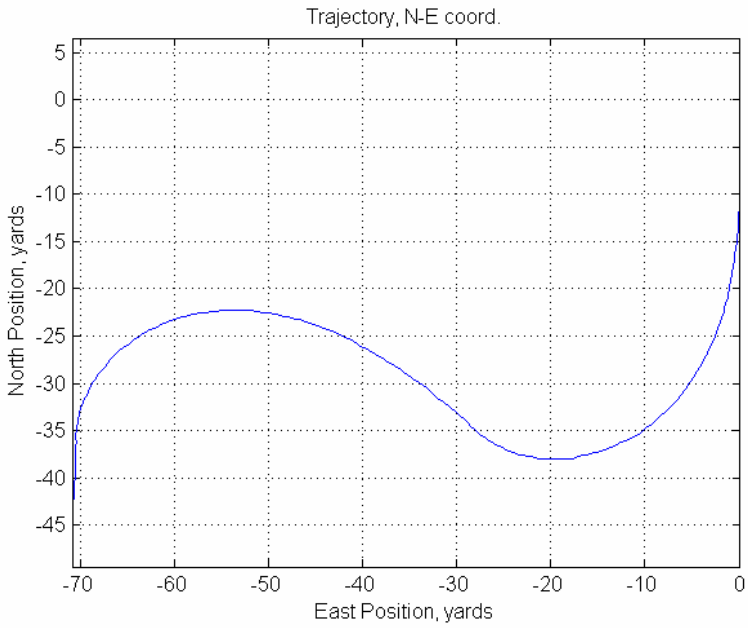

Figure 3.6: Tractor Position Trajectory

Figure 3.7 shows the configuration of the two load cells used to calculate the lateral force, F_{yh}. They are referred to as SU4 and SL5, respectively and are 20,000 lb cells that are positive in compression.

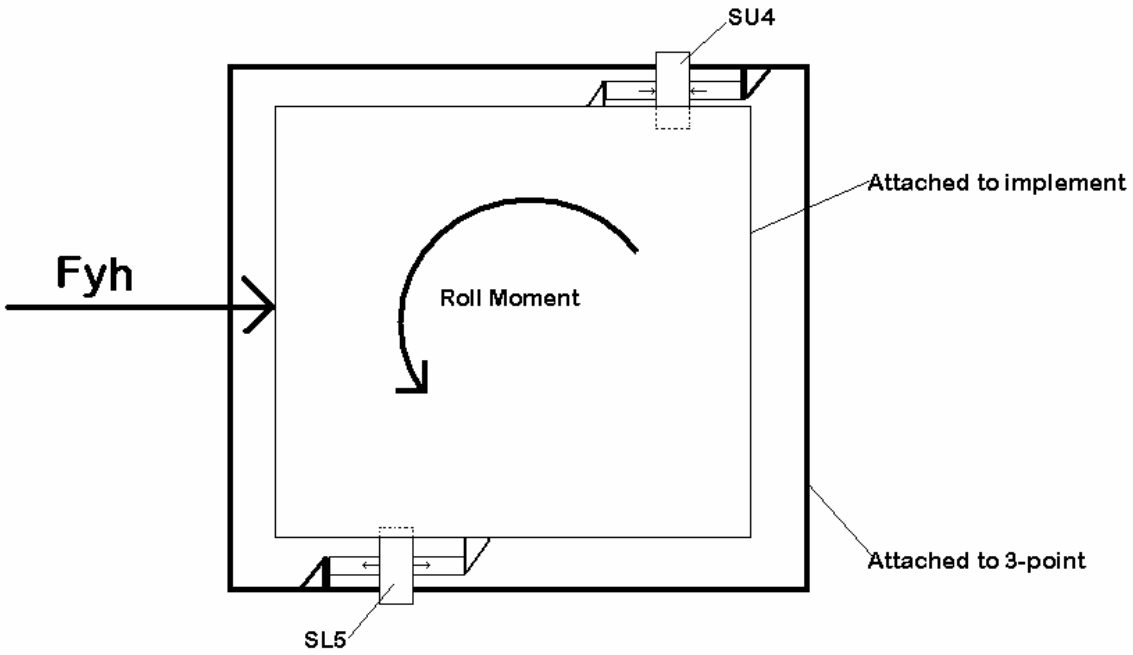

Figure 3.7: Diagram of Load Cells Measuring the Side Forces on USDA's Dyno

The F_{yh} shown in Figure 3.7 is in the positive direction for the "3-wheeled" Bicycle Model, with SL5 in tension and SU4 in compression. The roll moment on the dynomometer caused by the implement must be taken into consideration when using the data from these two load cells. This is due to the fact that the roll moment imparts a force into each of the cells. For a positive F_{yh}, the SU4 data will be positive and the SL5 data will be negative. A roll moment decreases the positive SU4 value and increases the negative SL5 value by the same amount. The lateral force, F_{yh}, is calculated according to Equation (3.16). The roll effect force cancels out because what was subtracted from SU4 has been added to SU5.

$$F_{yh} = SU4 - SL5 \tag{3.16}$$

Figure 3.8 is a graphical demonstration of how the roll moment cancels out when the measured F_{yh} is calculated.

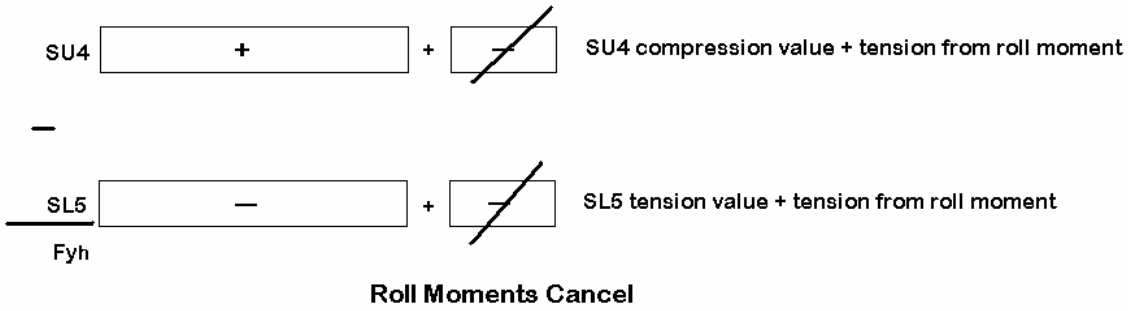

Figure 3.8: Roll Moment Effect in F_{yh} Calculations

Figure 3.9 shows the measured F_{yh} data obtained from the dynomometer on a particular data run. The lateral forces, as seen in the graph, increase with an increase in steering angle.

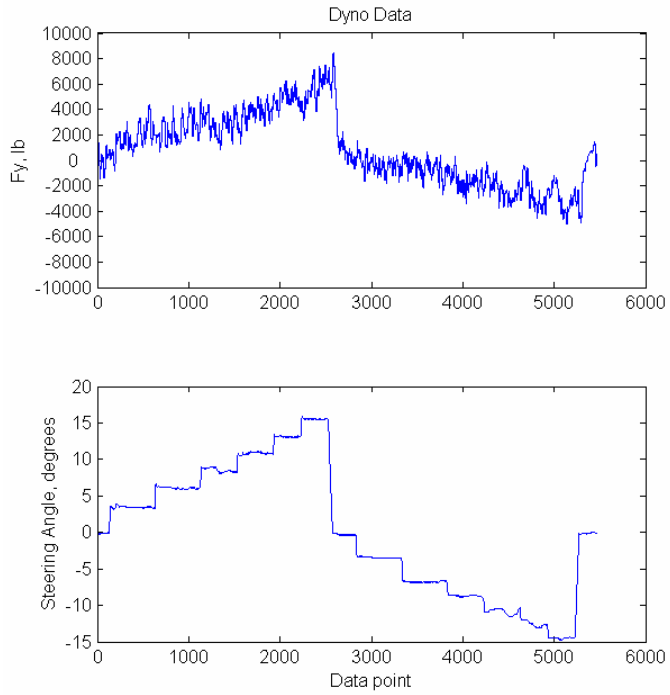

Figure 3.9: Lateral Force and Velocity taken from the Dyno

Slip angle data is also used for the hitch model validation. The slip angle for the implement is calculated using the GPS data and yaw gyro data according to Equations (3.17-3.20).

$$\beta = \gamma_{GPS} - \int r \tag{3.17}$$

$$V_y = V \cdot \sin(\beta) \tag{3.18}$$

$$V_{yh} = V_y + r \cdot (b + c) \tag{3.19}$$

$$\alpha_h = \tan^{-1}\left(\frac{V_{yh}}{V_x}\right) \tag{3.20}$$

Where γ_{GPS} is the GPS course measurement.

3.4 Hitch Model Validation

The collected force and slip angle data are compared in this section to determine if their relationship can be approximated by the linear tire model. Figures 3.10-3.12 show individual data runs of F_{yh} vs. slip angle for each depth at the test speed of 4 mph. Plots of the combined data runs fitted with a linear fit, for each depth respectively, are shown in Figures 3.13-3.15. Although the data runs show a high dispersion, a linear relationship in the data can still be seen. Figure 3.16 shows the data for each depth plotted together. Based on the linear fits of Figure 3.16, the slope $C_{\alpha h}$ increases with the depth of the implement as one would expect. This is due to the fact that as the depth increases, there is more resistance to turning, meaning that more lateral force is created for a given α_h per each depth respectively, and an increasing $C_{\alpha h}$.

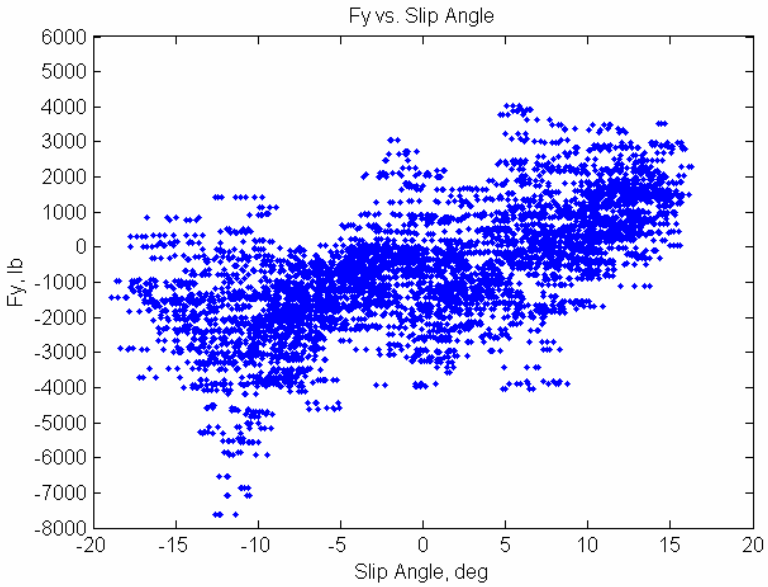

Figure 3.10: F_{yh} vs. Slip Angle at the Hitch for 6" Depth @ 4mph (individual run)

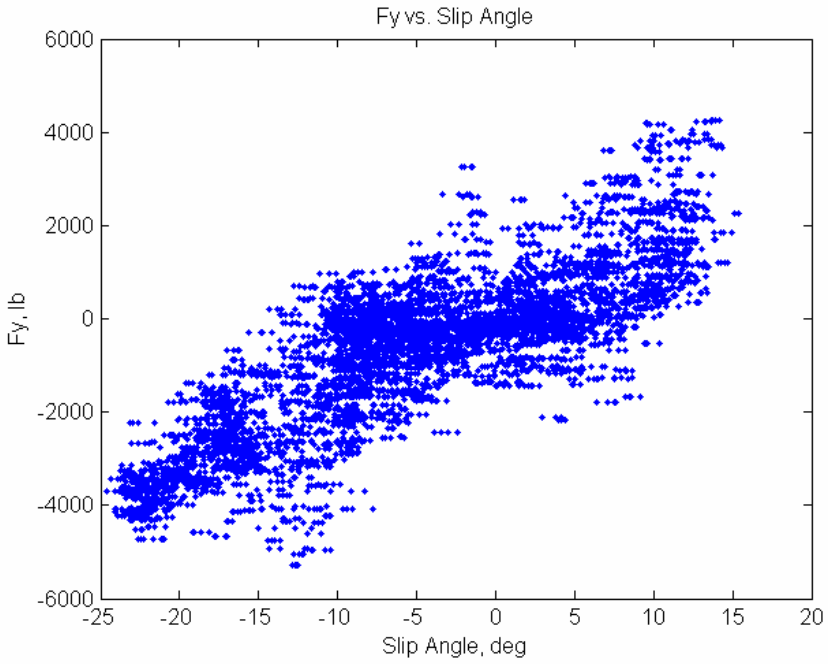

Figure 3.11: F_{yh} vs. Slip Angle at the Hitch for 12" Depth @ 4mph (individual run)

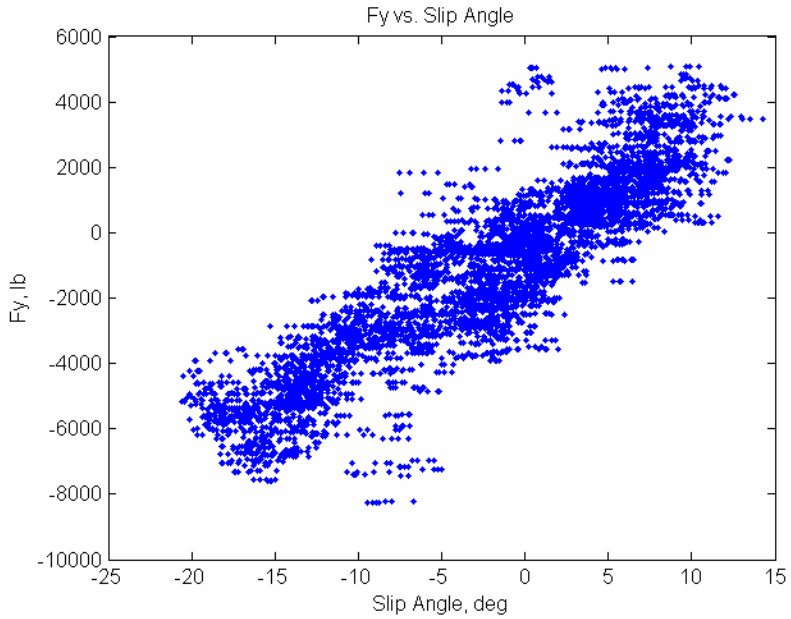

Figure 3.12: F_{yh} vs. Slip Angle at the Hitch for 18" Depth @ 4mph (individual run)

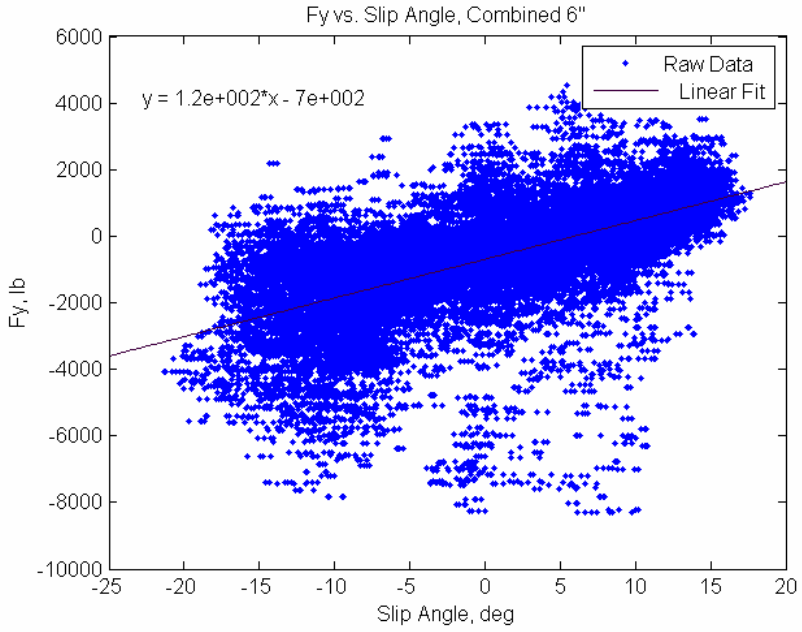

Figure 3.13: F_{yh} vs. Slip Angle at the Hitch for 6" depth @ 4mph (runs combined)

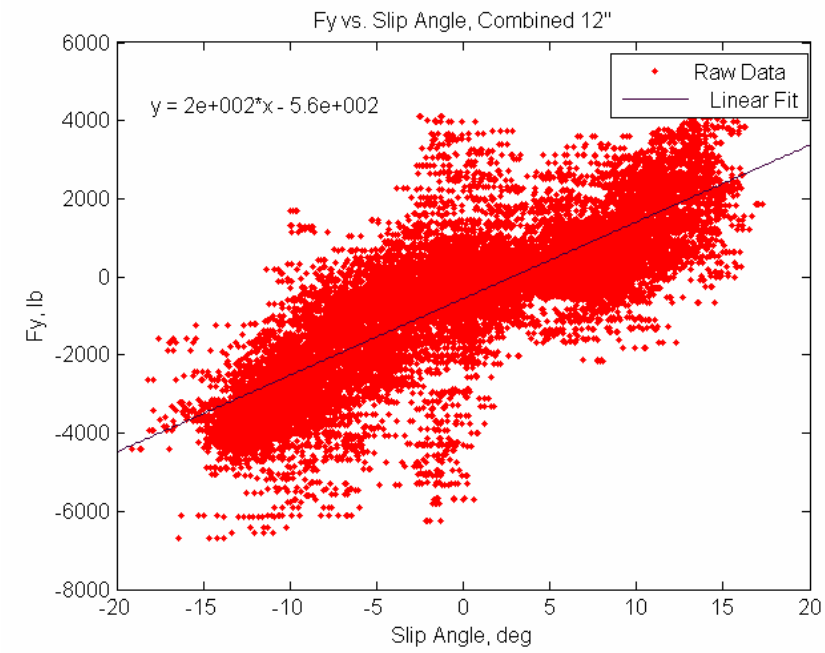

Figure 3.14: F_{yh} vs. Slip Angle at the Hitch for 12" depth @ 4mph (runs combined)

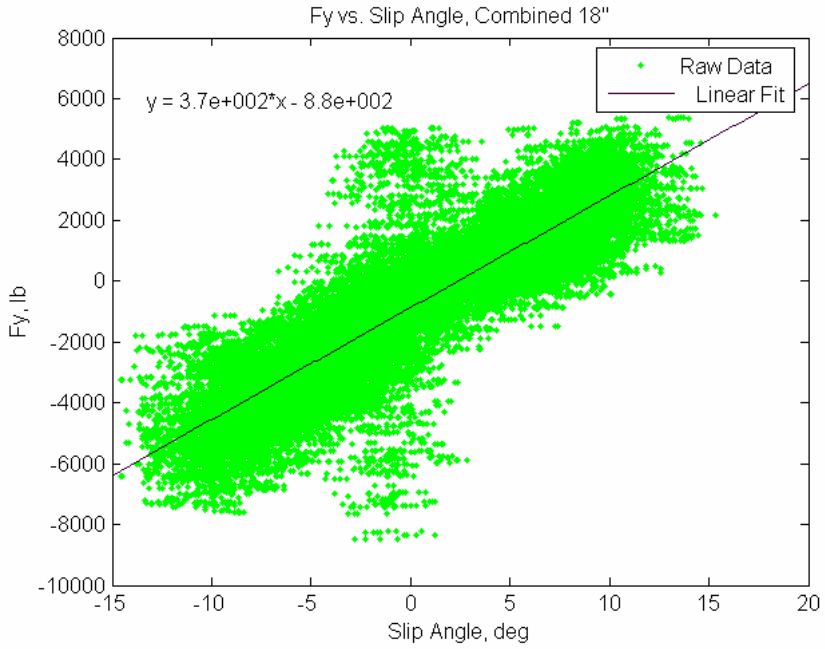

Figure 3.15: F_{yh} vs. Slip Angle at the Hitch for 18" depth @ 4mph (runs combined)

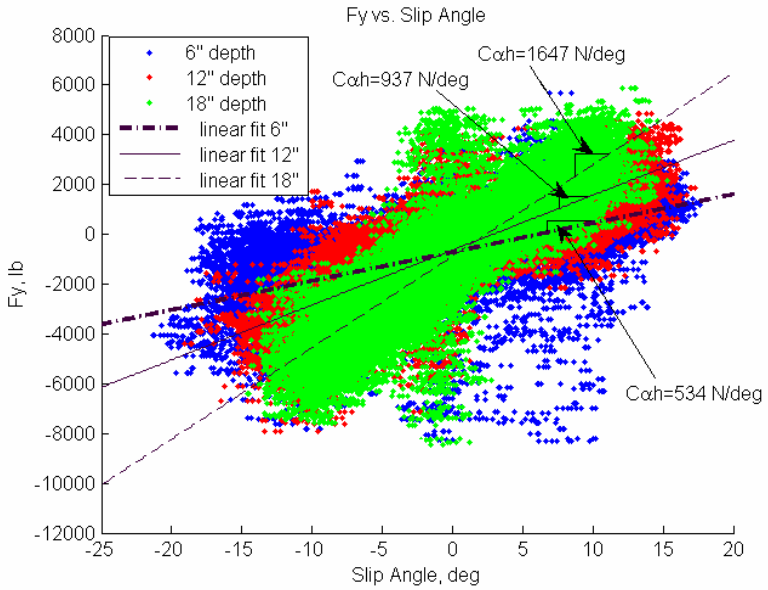

Figure 3.16: F_{yh} vs. Slip Angle at the Hitch for all depths @ 4mph

Table 3.1 lists the values of $C_{\alpha h}$ obtained for each depth using the dynamometer. It should be noted that these are empirically determined cornering stiffnesses strictly based on the slope of the fitted F_{yh} line of Figure 3.16.

Table 3.1: Empirically Determined $C_{\alpha h}$ Values on the 8420 with a Deere 955 4 Shank Ripper

Depth, inches	$C_{\alpha h}$, N/deg
6	534
12	937
18	1647

Comparing the lines of Figure 3.16 with Figure 3.3, the linear tire curve, it can be seen that the hitch forces do not peak, even at rather high slip angles like the tire forces do. This is most likely due to the fact that an implement has parts that actually stick into the ground instead of riding on top like a tire. Also, where relaxation lengths are concerned, a small relaxation length at the implement could occur due to slop in the 3 point hitch and/or from deformation of the dirt due to the geometry of the tine in the ground.

On a different note, the implement draft force, F_{xh}, can be seen to be a function of $C_{\alpha h}$, as shown in Figure 3.17 below. Moreover, it appears that there is a linear relationship between the two.

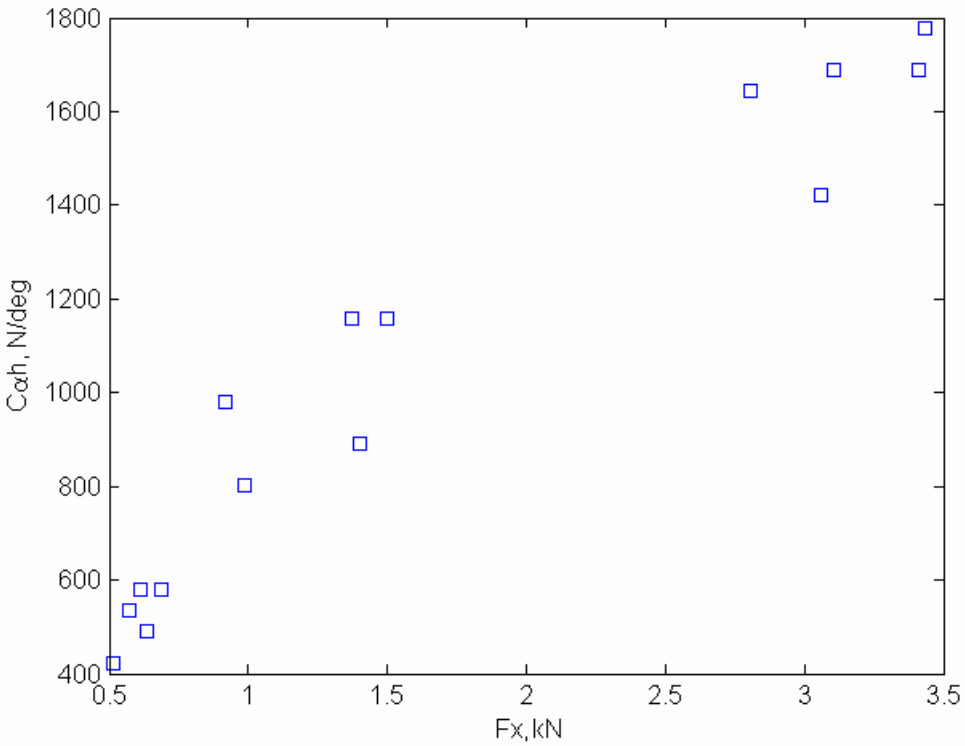

Figure 3.17: Correlation of Draft Force, F_{xh} with $C_{\alpha h}$ for the 4 Shank Ripper on the 8420

3.5 Differential Hitch Forces

The data used to validate the F_{yh} model can also be used to look at the moment created from differential hitch forces. Figure 3.18 below shows the moment from the lateral force about the tractor's center of gravity, M_{CG} from Equation (3.13), compared with the moment caused by the differential forces, M_{diff} from a dyno run at a depth of 18" on the four shank ripper. Figure 3.19 shows a run at 12". As can be seen in the figures, the moment acting upon the tractor is dominated by the moment from the lateral force. The data are similar for all runs at 18" and for all runs at 12". Based on these

results, the moment from the differential forces at the hitch is negligible compared to the effect of the lateral force moment, and neglecting M_{diff} in the "3-wheeled" Bicycle Model structure will not significantly affect its performance. This validation is also true for the "3-wheeled" FHRL Model because it uses the "3-wheeled" Bicycle Model in its structure.

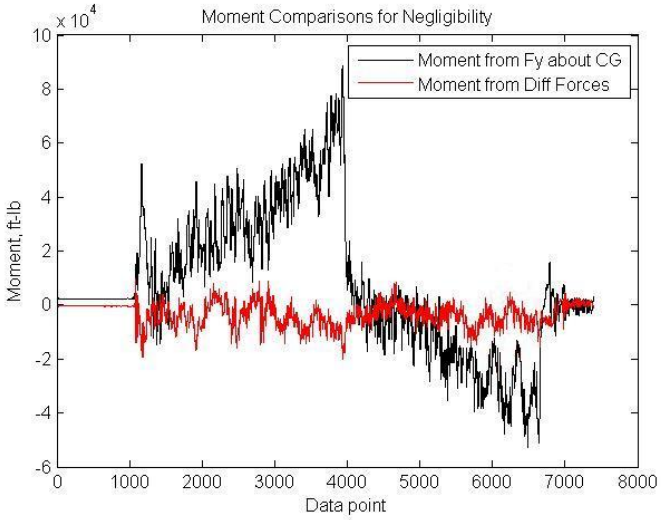

Figure 3.18: Yaw Moment from F_{yh} about CG vs. Moment from Diff Forces at 18"

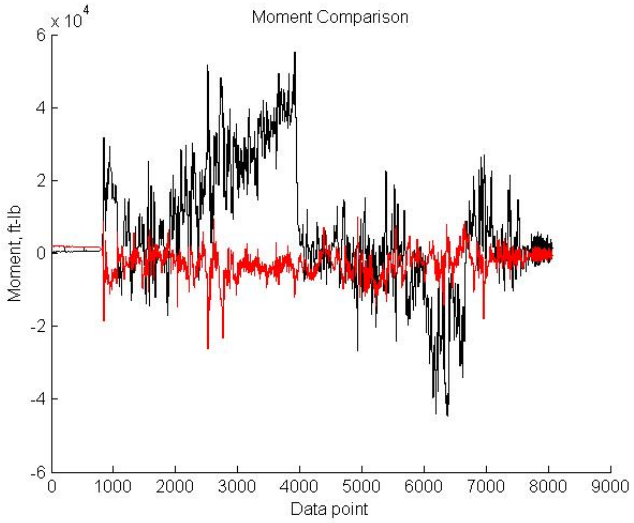

Figure 3.19: Yaw Moment from F_{yh} about CG vs. Moment from Diff Forces at 12”

3.6 Conclusions

This chapter provides a more in depth derivation of the hitched implement model. It has been shown through the lateral force vs. slip angle data that the implement can be modeled as a linear tire. It has also been shown through experimental data that the moments due to differential longitudinal loading on the implement are negligible compared to the lateral implement forces. Therefore, this chapter has shown that the “3-wheeled” bicycle model, developed in the previous chapter, accurately represents the hitched implement and makes reasonable assumptions about the hitched implement model.

CHAPTER 4

SOLVING OF PARAMETERS WITH SYSTEM IDENTIFICATION

4.1 Introduction

This chapter validates the models chosen in the previous chapter against the real tractor. Two types of data have been collected on a variety of implements at varying depths and speeds for this purpose: DC gain data and dynamic chirp data. The DC gain data is used in conjunction with the "3-wheeled" Bicycle Model to solve for the ranges in $C_{\alpha h}$ with each implement and depth. The chirp data is used to create a system identification model in order to compare the dynamics of the "3-wheeled" Front and Hitch Relaxation Length (FHRL) Model and validate that it captures the critical dynamic responses of the real system. The front and hitch relaxation lengths are also solved for using the dynamic response data.

4.2 Data Collection

A John Deere 8420 tractor with single rear wheels and also a Deere 8520 with dual rear wheels were used to gather the DC gain and dynamic data. The experimental setup for these experiments is detailed in Appendix A. Table 4.1 lists the depths and speeds for data collected on a four shank ripper with the 8420. Table 4.2 lists the depths,

speeds, and implements for the data that was taken on the 8520. The implements used with the 8520 were a 5 shank ripper, an 18 bottom cultivator, an 11 row bedder, and the bedder out of the ground. The difference in using a single vs. dual wheel tractor for experiments is that the rear tire cornering stiffness is doubled because the dual rear wheel tractor has twice as many tires.

Table 4.1: Data Collection, 8420

Implement: 4 Shank Ripper	Speed, mph						
Depths: 4, 8, 12”	2.5	3	3.5	4	4.5	5	5.5

Table 4.2: Data Collection, 8520

Implement	Depth at Given Speed			
	1 mph	2.5 mph	4 mph	5.5 mph
Bedder Out of Gnd	--	--	--	--
11 Row Bedder	9”	9”	9”	9”
18 Bottom Cultivator	9”	9”	9”	9”
5 Shank Ripper	10, 15, 20”	10, 15, 20”	10, 15, 20”	10, 15, 20”

The DC gain experiments consisted of a series of steady state step steering inputs of increasing magnitude to create a series of steady state step yaw outputs. Using these experiments, the DC gain from steady state steer angle to steady state yaw rate is identified empirically. Figure 4.1 shows the steering angle and resulting yaw rate of a typical DC gain run at a speed of 2.5 mph.

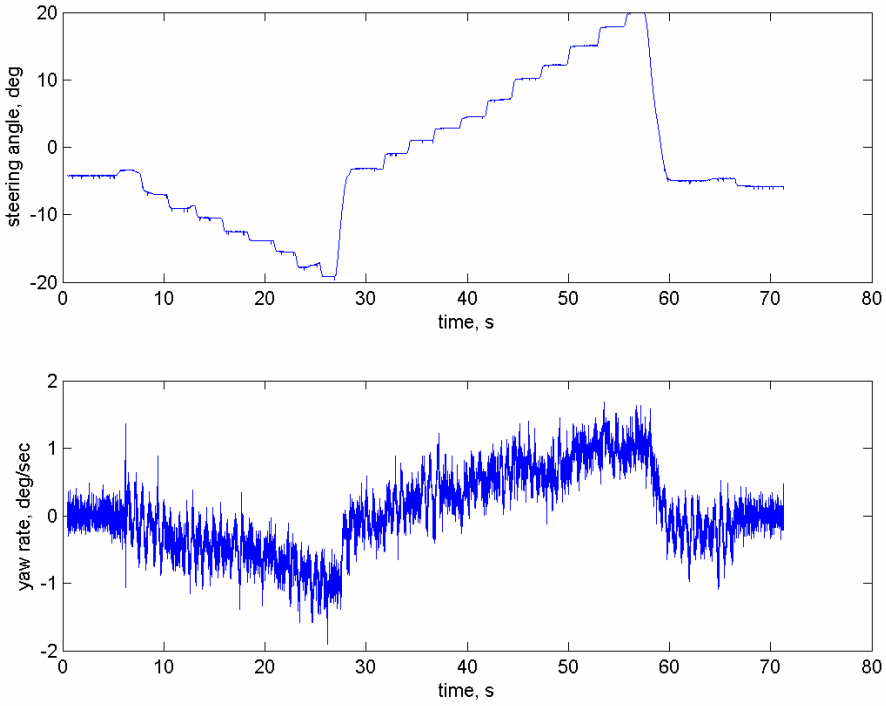

Figure 4.1: Steering Angle Profile and Yaw Rate Response for DC Gain Experiment

While a steady state step steering input is useful for identifying the steady state characteristics, a chirp steering input is useful for identifying the dynamic response of the tractor [14]. A chirp steering input consists of applying a sine wave of increasing frequency to the steering wheels. Figure 4.2 shows a typical chirp steering angle profile and resulting yaw rate for the dynamic response experiments. As can be seen, the steering angle is not a true chirp signal at the wheels, which does affect the system identification. This is most likely due to the steering servo and hydraulic system on the tractor not being able to react fast enough to create a true chirp signal at high frequencies.

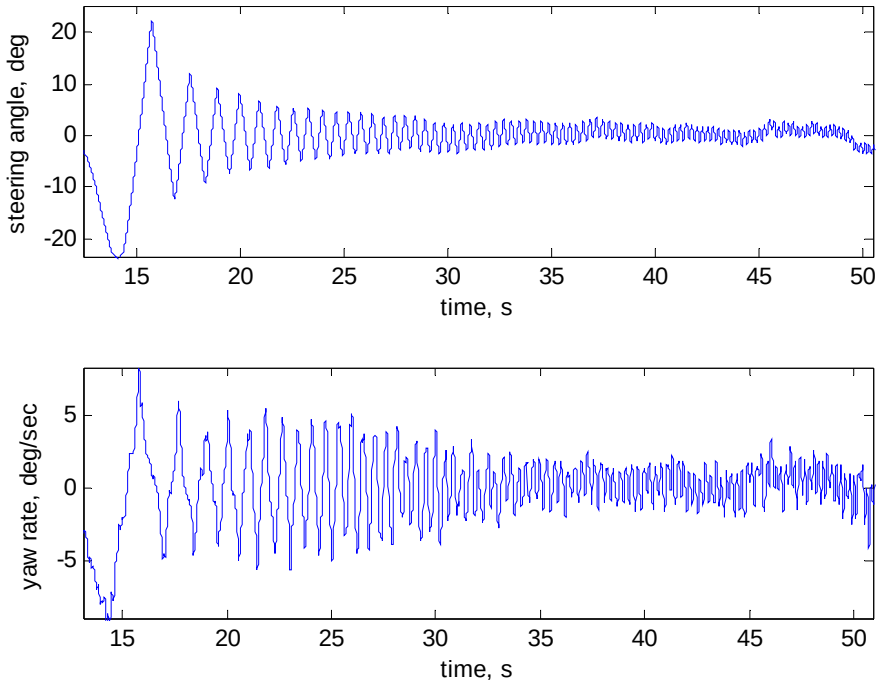

Figure 4.2: Steering Angle Profile and Yaw Rate Response for Dynamic Chirp Experiment

4.3 DC Gain Response

4.3.1 Empirical DC Gain

The steering angle input and the yaw rate output from the steady state data is used to find the empirical DC gain of the system. Least squares fits are performed to determine the empirical DC gain of the system at each depth over the range of speed at that depth for each implement [15]. Equation (4.2) models the measured yaw rate as a function of DC gain times steering angle, a gyro bias, and white noise.

$$r_{meas} = G_{DC} \cdot \delta + r_{bias} + noise \tag{4.2}$$

Note that Equation (4.2) is only valid in steady state. The DC gain and gyro bias were identified using recorded steering angles and yaw rates for each configuration and speed.

After the DC gain is identified, it can be validated by comparing the fit to the measured response. Figure 4.3 shows a typical result for this validation. The fit from Figure 4.3 has an RMS error of .1726 deg/sec, where the sensor noise is the largest contributor to the magnitude of the RMS error.

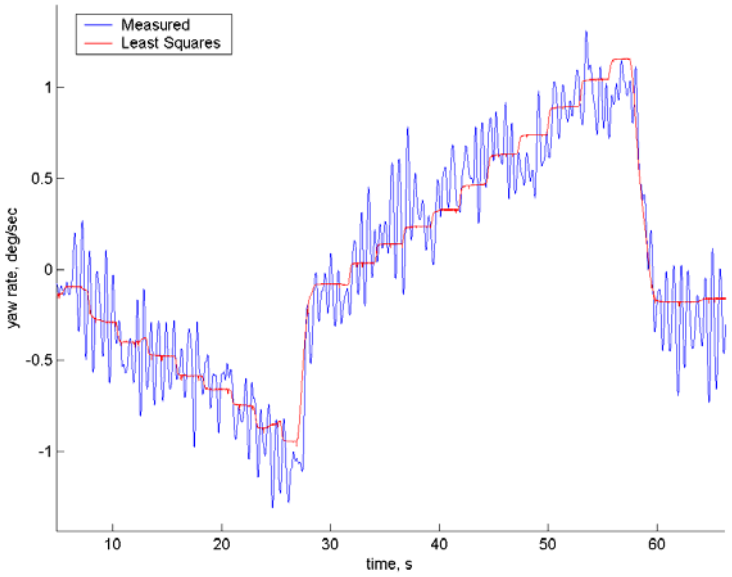

Figure 4.3: Least Squares Fit of the Steady State Yaw Rate

The empirical DC gain fits obtained for the 8420 and four shank ripper at three different depths are shown in Figure 4.4. Figure 5.5 shows the empirical DC gain fits for all the implements, depths, and speeds with the 8520.

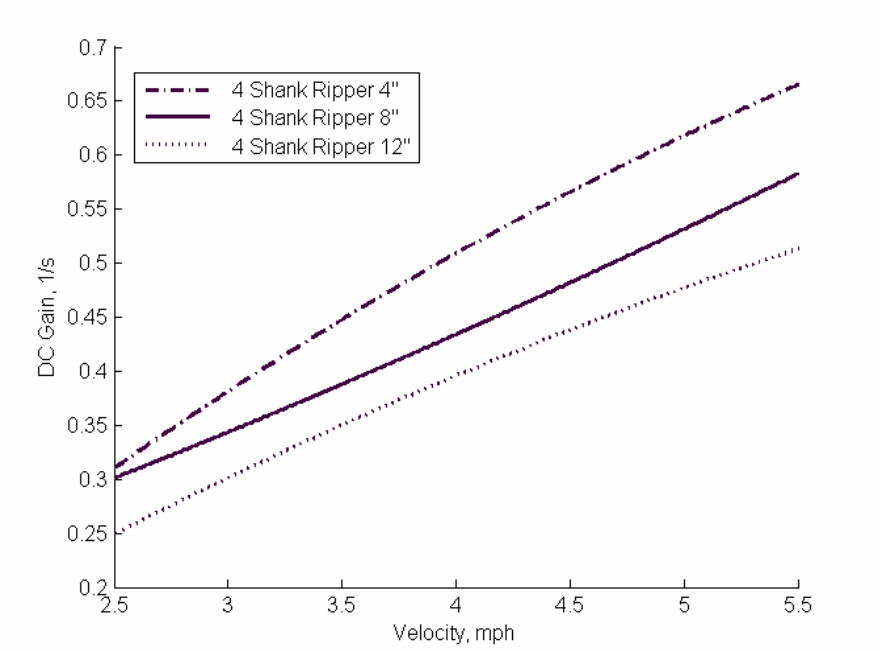

Figure 4.4: Empirically Determined DC Gain for All Depths, 8420 with Four Shank Ripper

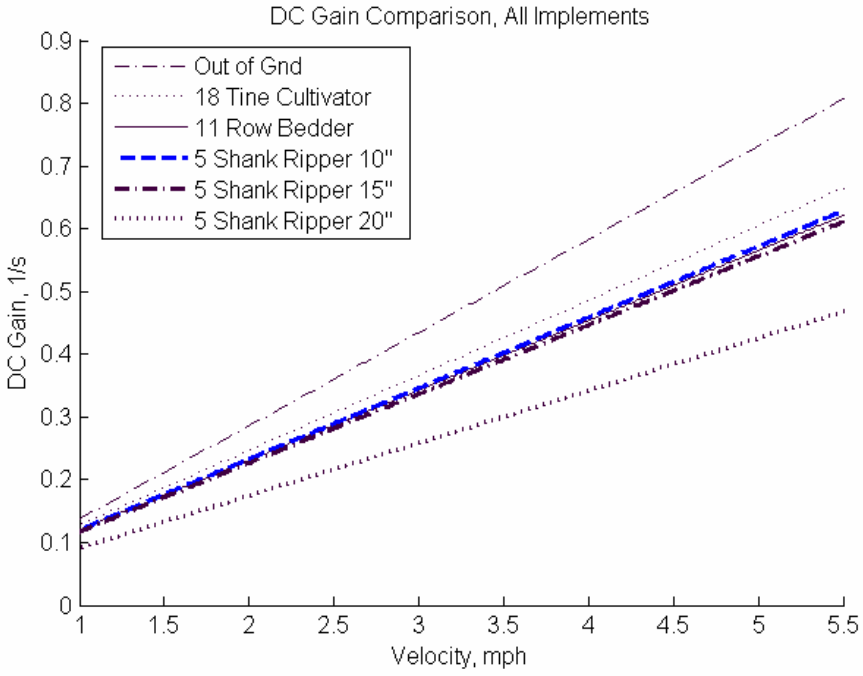

Figure 4.5: Empirically Determined DC Gain for All Implements at All Depths, 8520

4.3.2 Solving of $C_{\alpha h}$

Once the empirical DC gains for each implement, depth, and velocity are found, the $C_{\alpha h}$ which best fits empirical DC gain values is found. Equation (4.2) is an analytical equation for the DC gain and is derived from Equation (2.33) of the "3-wheeled" Bicycle Model.

$$Gdc = \frac{\frac{C_{\alpha f} \cdot C_1 + C_{\alpha f} a \cdot C_2}{mV}}{\frac{(C_3) \cdot (C_2) - (C_1)^2}{mV^2} + (C_1)} \tag{4.2}$$

Where C_1, C_2, and C_3 were defined previously in Equation (2.34), but are shown below for reference.

$$C_1 = ((b+c) \cdot C_{\alpha h} + b \cdot C_{\alpha r} - a \cdot C_{\alpha f})$$

$$C_2 = \left(C_{\alpha h} + C_{\alpha r} + C_{\alpha f}\right)$$

$$C_3 = ((b+c)^2 C_{\alpha h} + C_{\alpha r} b^2 + C_{\alpha f} a^2)$$

The above equation for DC gain is only a function of $C_{\alpha h}$ and velocity since the other parameters are already known. Therefore, $C_{\alpha h}$ can be solved for by numerically minimizing Equation (4.3).

$$E = \frac{1}{N} \cdot \left(\sum_{1}^{N} (Gdc\_empirical(N) - Gdc(C_{\alpha h}))^2 \right)^{1/2} \tag{4.3}$$

Figure 4.6 shows the results of the minimization for the four shank ripper used on the 8420. The values obtained for $C_{\alpha h}$ at each depth are also shown: 451.65 N/deg at four

inches, 1002.8 N/deg at eight inches, and 1719.3 N/deg at twelve inches of depth. Figure 4.7 and 4.8 show the results from the implements used on the 8520. The $C_{\alpha h}$ values obtained on the five shank ripper are: 887.3 N/deg at ten inches, 1025 N/deg at fifteen inches, and 3385.3 N/deg at twenty inches of depth. The value obtained for the bedder out of the ground is .983 N/deg, which is approximately 0, as should be in the case where there is no cornering stiffness from the implement. The value obtained for the eighteen tine cultivator is 639.8 N/deg, and the value for the eleven row bedder is 951.2 N/deg. The large jump in $C_{\alpha h}$ at the deepest depth in Figure 4.7 may be due to variation in soil compaction.

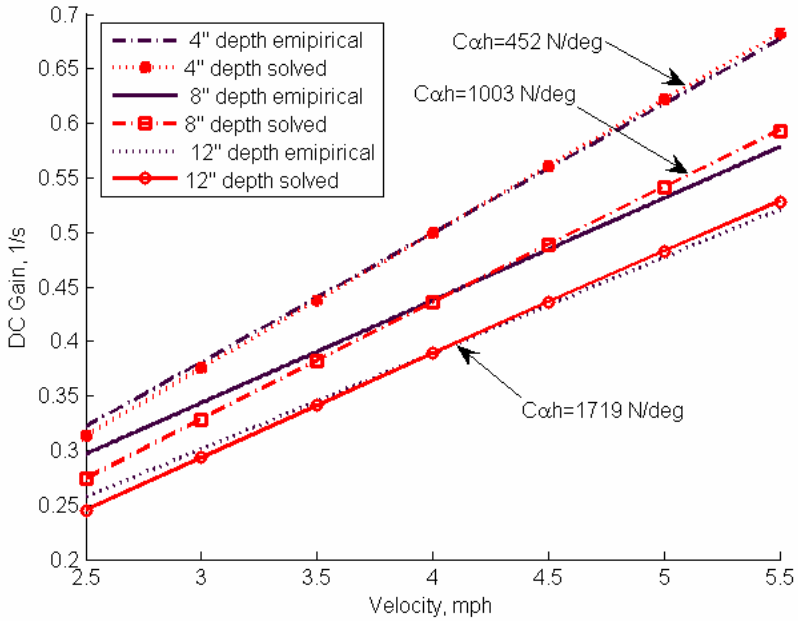

Figure 4.6: Empirical and Solved DC Gain Comparison for the 4 Shank Ripper on the 8420 at Various Depths

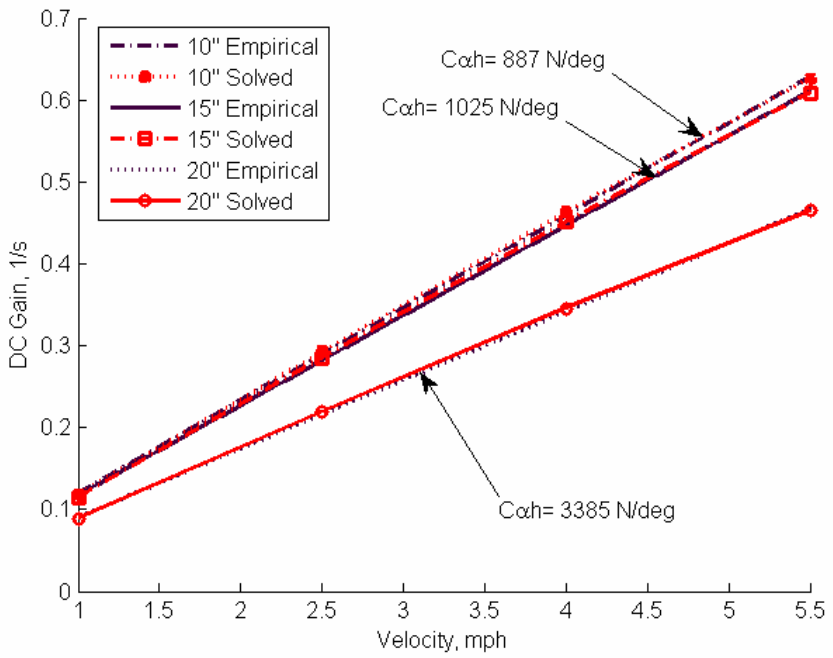

Figure 4.7: Empirical and Solved DC Gain Comparison for the 5 Shank Ripper on the 8520 at Various Depths

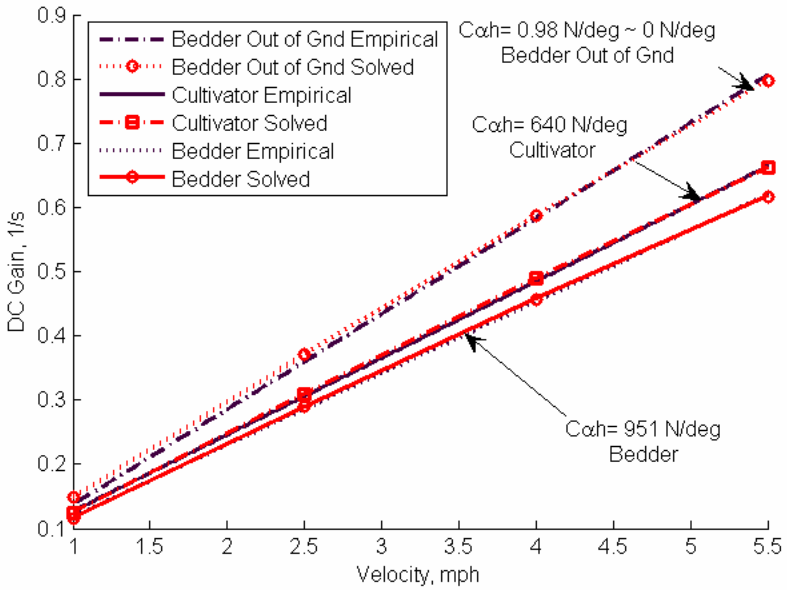

Figure 4.8: Empirical and Solved DC Gain Comparison for the Bedder out of the Ground, the Bedder in the Ground, and the Cultivator on the 8520.

Based on Figures 4.6-4.8, a trend in the value of the hitch cornering stiffness can be seen. As would be expected, the cornering stiffness increases with the size of the implement and also with the depth of each implement respectively. Additionally, $C_{\alpha h}$ increases with the draft load as shown by Figure 3.17. This trend corresponds to an implement providing a greater resistance to turning the deeper that it is in the ground and also corresponds to an implement with more or larger tines in the ground being harder to turn.

Table 4.3 summarizes the values of $C_{\alpha h}$ obtained for all of the implements and their respective depths.

Table 4.3: Empirically Determined $C_{\alpha h}$ Values for all the Implements

Implement	Depth, inches	$C_{\alpha h}$, N/deg
8420, 4 Shank Ripper	4	451.65
8420, 4 Shank Ripper	8	1002.80
8420, 4 Shank Ripper	12	1719.30
8520, Bedder Out of Gnd	0	0.98 ~ 0.00
8520, Cultivator	9	639.83
8520, Bedder	9	951.24
8520, 5 Shank Ripper	10	887.33
8520, 5 Shank Ripper	15	1025.00
8520, 5 Shank Ripper	20	3385.30

4.4 Dynamic Response: Empirical Modeling

The interpretation and results from using the dynamic chirp input and output responses of Figure 4.2 and from the implements and depths of Tables 4.1 and 4.2 are discussed in this section.

Experiments using a chirp input are useful for determining the dynamic characteristics of a system since the chirp signal excites a range of frequencies. This allows the magnitude and phase shift of the output vs. the input over that range of frequencies to be analyzed. This can be accomplished by taking an Empirical Transfer Function Estimate (ETFE) of the data sets using Matlab's "etfe( )" command [14]. Figure 4.9 shows an ETFE for the cultivator at a speed of one mile per hour. The large jump in noise in the graph past 100 rad/s is due to lack of input excitation frequency. This ETFE represents the general shape and form for all of the data sets recorded.

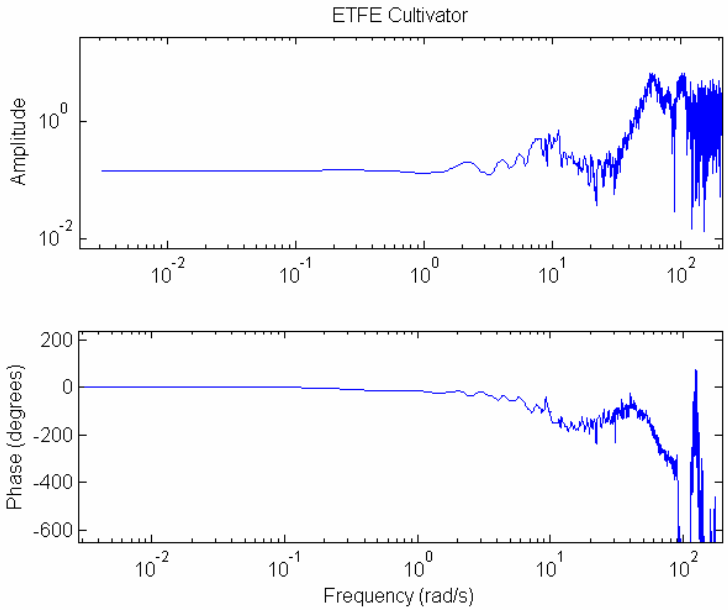

Figure 4.9: ETFE of the Cultivator at 1 mph

Since the ETFE is a purely empirical model, a system identification model is fitted for each ETFE. For this research, a Box Jenkins model was chosen for the system identification model [16]. $G(s)$ of Equation (4.4) represents the real tractor system, while the Box Jenkins models represents $\hat{G}(s)$, the approximated system.

$$\frac{r(s)}{\delta(s)} = \hat{G}(s) \tag{4.4}$$

Figure 4.10 shows the ETFE of the four shank ripper with a fourth order Box Jenkins identified model plotted alongside. Fourth order Box Jenkins models were found to best fit the data sets in Tables 4.1 and 4.2. The first resonant peak of Figure 4.10 represents the dominant dynamics of the tractor (which is of most interest); it is uncertain what dynamics are creating the second resonance. Both test tractors had an independent front suspension which may be causing this second resonance.

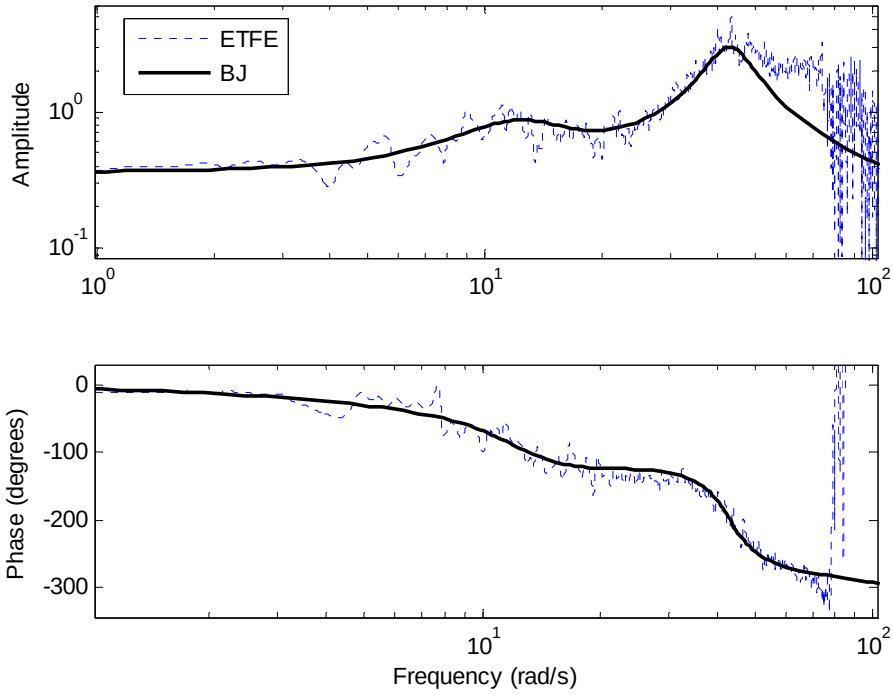

Figure 4.10: ETFE of the 4 Shank Ripper with 4th order Box Jenkins

Figures 4.11-4.19 show plots of the empirical DC gains, natural frequencies, and damping ratios vs. velocity of the tractor-implement combination calculated from the Box Jenkins Models. It should be noted that the natural frequencies and damping ratios are those associated with the first resonant peaks. These figures also show the analytical values attained by adjusting the front and hitch relaxation lengths of the "3-wheeled" FHRL Model. Recall, however, that the DC gain values are not a function of the relaxation lengths. The DC gain values are for reference only and are the values shown for the empirical gains in the previous section.

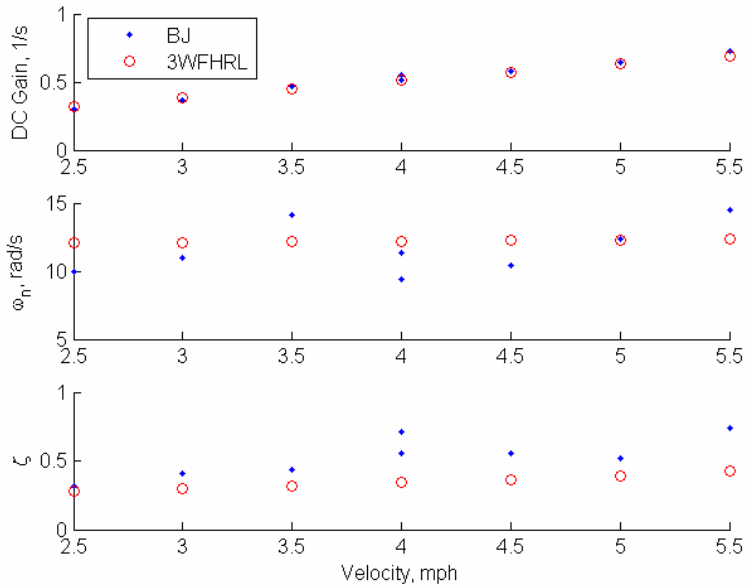

Figure 4.11: DC Gain, Natural Frequency, and Damping Ratio for the 4 Shank Ripper at 4" of depth on the 8420, $\sigma_f = .4\,\text{m}$, $\sigma_h = .002\,\text{m}$

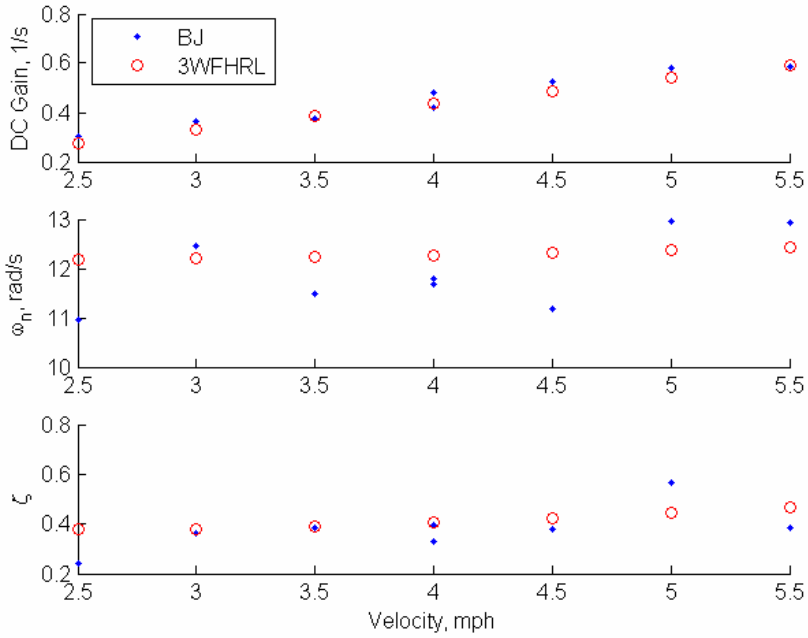

Figure 4.12: DC Gain, Natural Frequency, and Damping Ratio for the 4 Shank Ripper at 8" of depth on the 8420, $\sigma_f = .4\,\text{m}$, $\sigma_h = .002\,\text{m}$

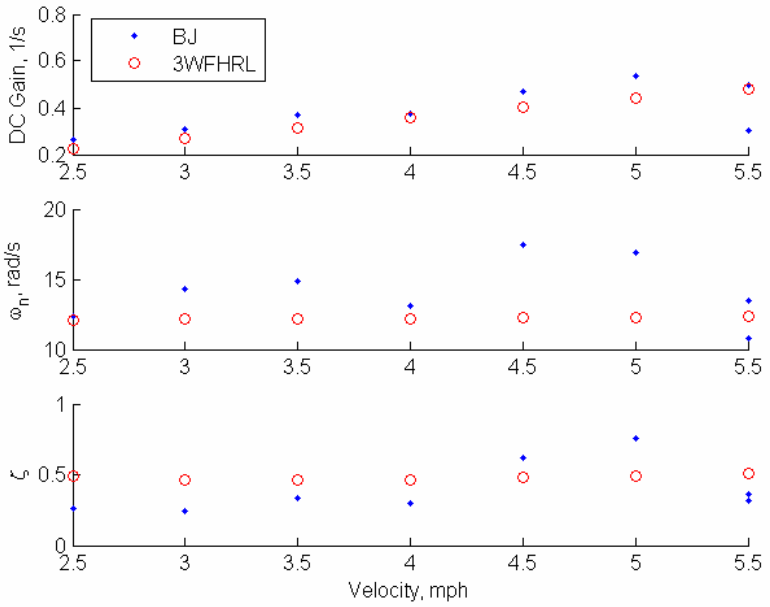

Figure 4.13: DC Gain, Natural Frequency, and Damping Ratio for the 4 Shank Ripper at 12" of depth on the 8420, $\sigma_f = .4\,\text{m}$, $\sigma_h = .002\,\text{m}$

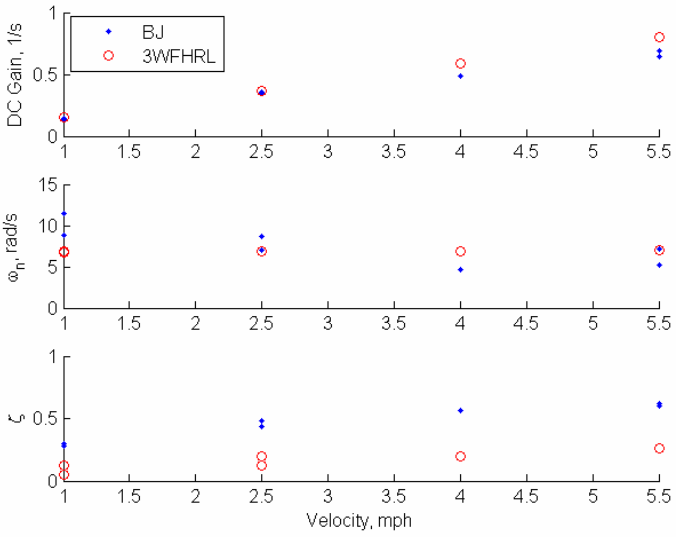

Figure 4.14: DC Gain, Natural Frequency, and Damping Ratio for the Bedder out of the Ground on the 8520, $\sigma_f = .9\,\text{m}$, $\sigma_h = .002\,\text{m}$

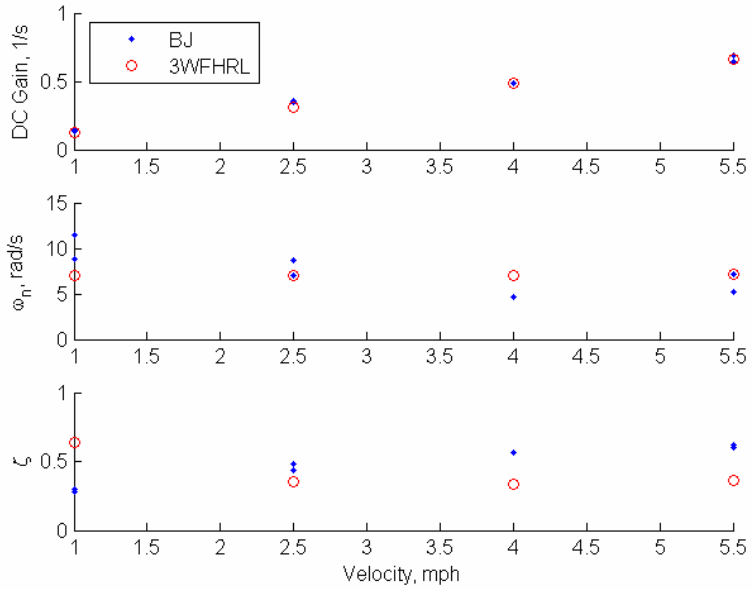

Figure 4.15: DC Gain, Natural Frequency, and Damping Ratio for the Cultivator on the 8520, $\sigma_f = .9\,\text{m}$, $\sigma_h = .002\,\text{m}$

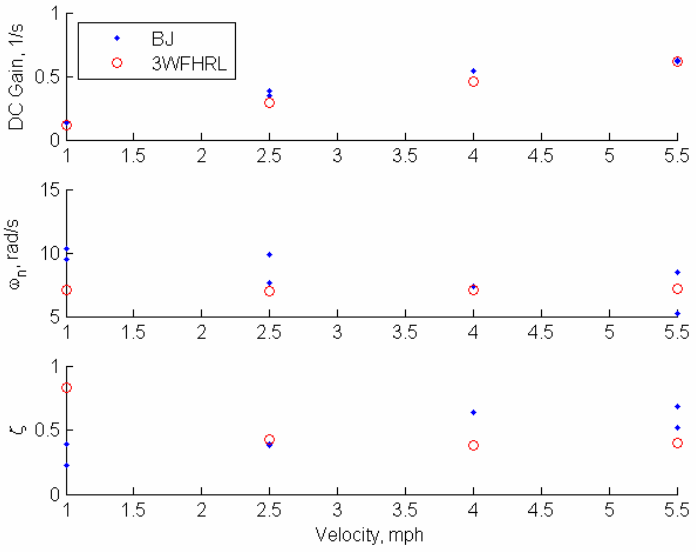

Figure 4.16: DC Gain, Natural Frequency, and Damping Ratio for the Bedder on the 8520, $\sigma_f = .9\,\text{m}$, $\sigma_h = .002\,\text{m}$

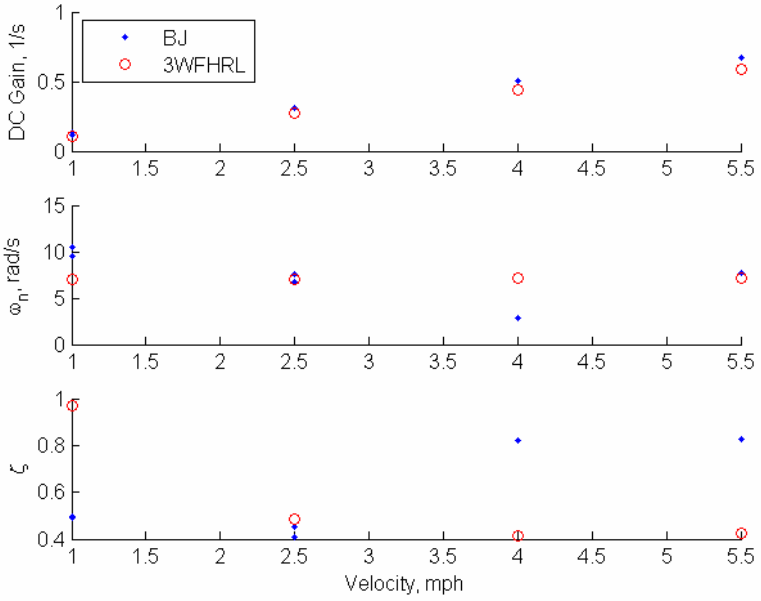

Figure 4.17: DC Gain, Natural Frequency, and Damping Ratio for the 5 Shank Ripper at 10” depth on the 8520, $\sigma_f = .9\,\text{m}$, $\sigma_h = .002\,\text{m}$

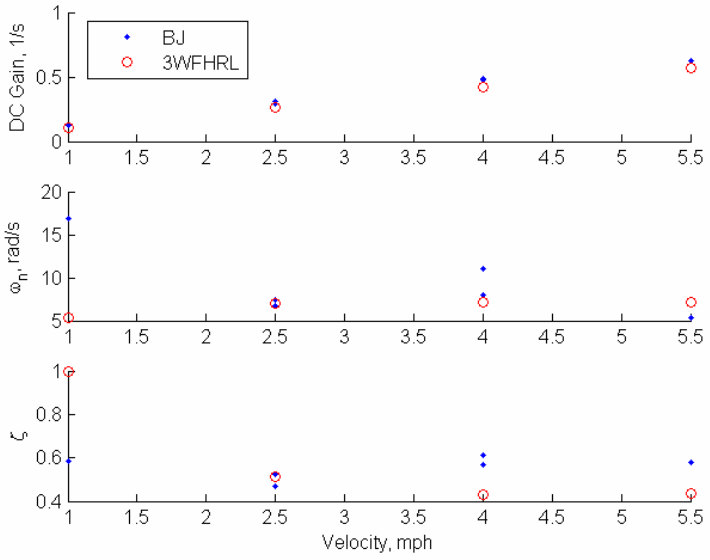

Figure 4.18: DC Gain, Natural Frequency, and Damping Ratio for the 5 Shank Ripper at 15” depth on the 8520, $\sigma_f = .9\,\text{m}$, $\sigma_h = .002\,\text{m}$

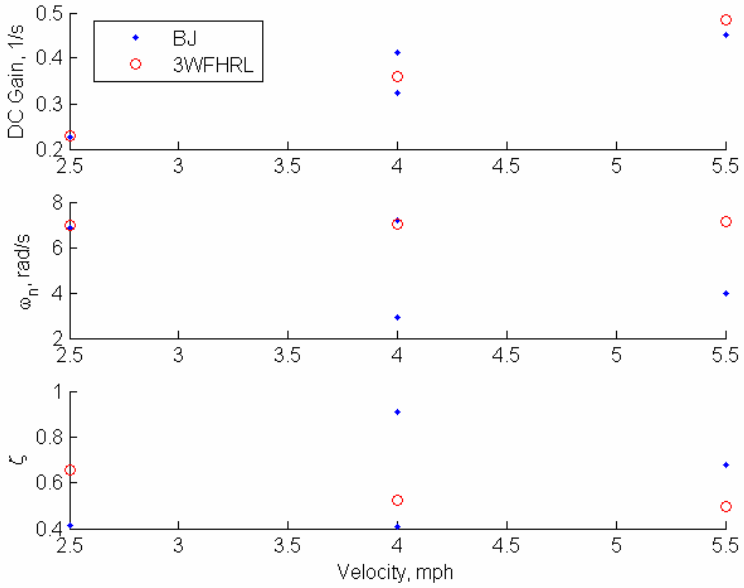

Figure 4.19: DC Gain, Natural Frequency, and Damping Ratio for the 5 Shank Ripper at 20" depth on the 8520, $\sigma_f = .9\,\text{m}$, $\sigma_h = .002\,\text{m}$

The resulting values for the front and hitch relaxation lengths are summarized in Table 4.4, below. The value of the front relaxation length for the four shank ripper at all depths on the 8420 was a lower value than that needed for the 8520 at all its implements and depths.

Table 4.4: Front and Hitch Relaxation Length Values

Tractor, All Implements	Front Relaxation Length Value (m)	Hitch Relaxation Length Value (m)
8420	.9	.002
8520	.4	.002

Although the relaxation lengths given in Table 4.3 match the experimental natural frequency, they do not capture the experimental trend in damping ratio. Additionally, these relaxation length values led to an RMS error (between experimental and model yaw rates) of 1.92 deg/s when analyzed in the same manner as Figure 2.12. Figure 4.20 shows the Bode velocity response of the "3-wheeled" FHRL Model at these relaxation length values, and it can be seen that the damping decreases with velocity, which is opposite of what Figures 4.11-4.19 denote.

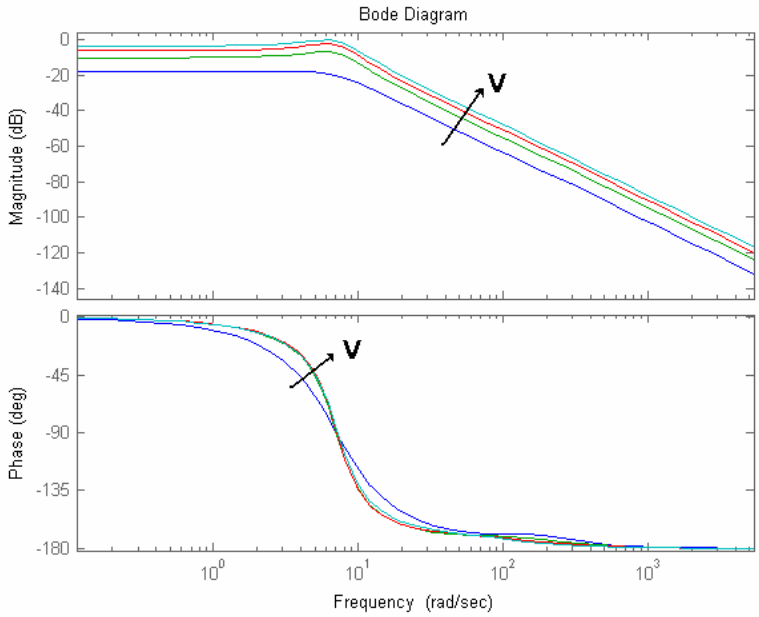

Figure 4.20: "3-wheeled" FHRL Model for the Cultivator on the 8520, $\sigma_f = .9\,\text{m}$, $\sigma_h = .002\,\text{m}$

This problem was remedied by using the relaxation length values that were used to obtain an RMS error of .67457 for Figure 2.12. These values are $\sigma_f = .37\,\text{m}$ and $\sigma_h = .4\,\text{m}$. Using these values in the "3-wheeled" FHRL Model also produces damping

that increases with velocity, seen in the Bode plots of Figure 4.21. Shown in Figures 4.22-30 are the DC gain, natural frequency, and damping ratio comparisons for all of the data sets. As seen in these figures, using values of .37 and .4 m for the front and hitch relaxation lengths yields natural frequencies that are relatively close to the values from the experimental fits.

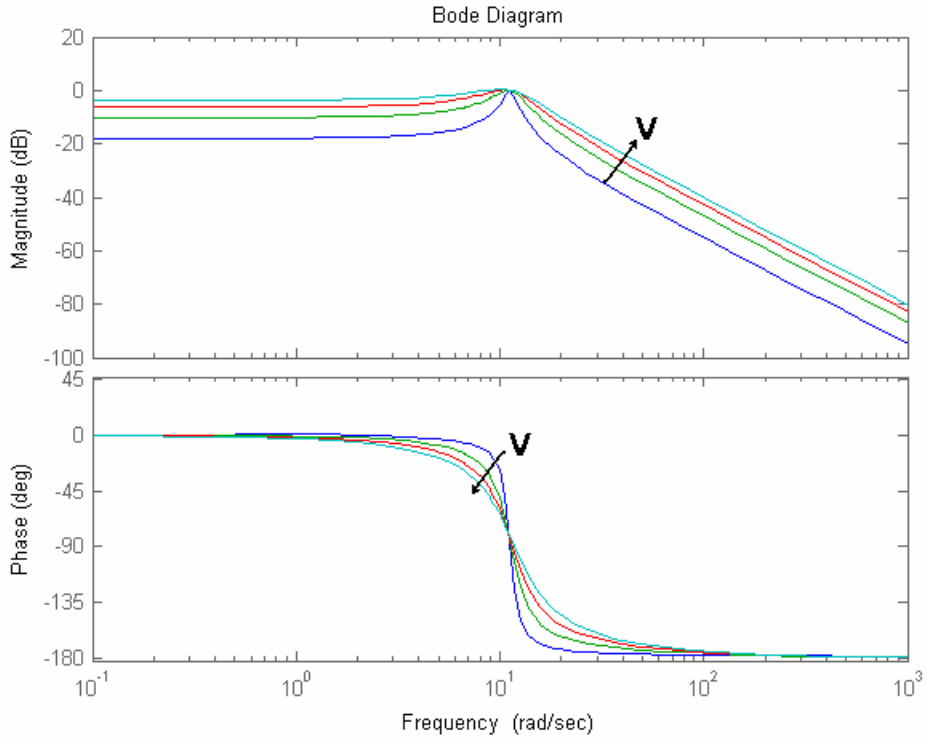

Figure 4.21: "3-wheeled" FHRL Model for the Cultivator on the 8520, $\sigma_f = .37$ m, $\sigma_h = .4$ m

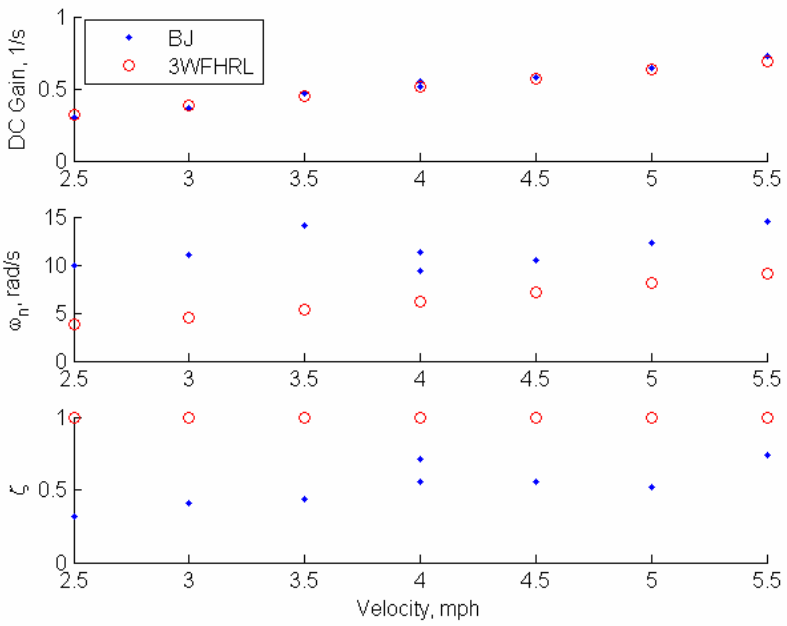

Figure 4.22: DC Gain, Natural Frequency, and Damping Ratio for the 4 Shank Ripper at 4" of depth on the 8420, $\sigma_f = .37$ m, $\sigma_h = .4$ m

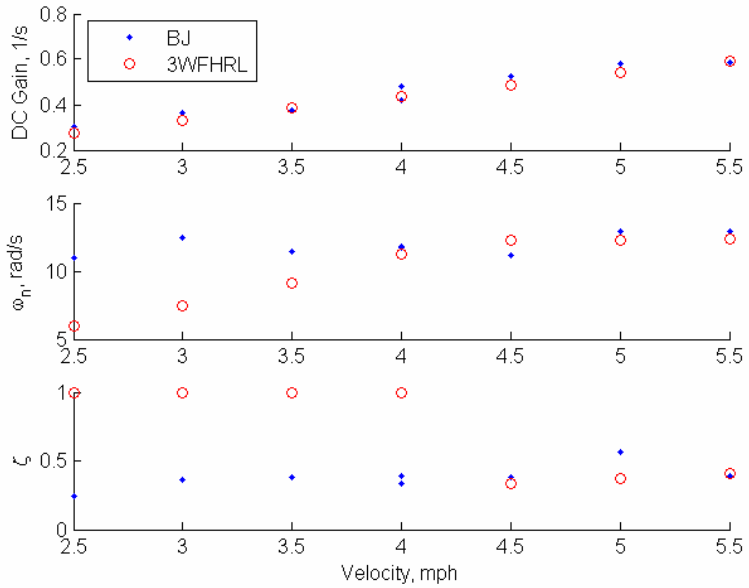

Figure 4.23: DC Gain, Natural Frequency, and Damping Ratio for the 4 Shank Ripper at 8" of depth on the 8420, $\sigma_f = .37$ m, $\sigma_h = .4$ m

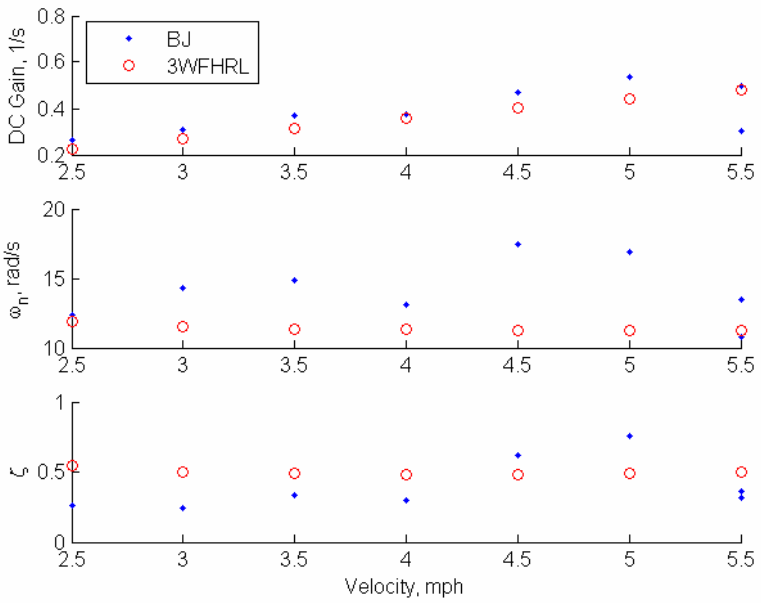

Figure 4.24: DC Gain, Natural Frequency, and Damping Ratio for the 4 Shank Ripper at 12” of depth on the 8420, $\sigma_f = .37$ m, $\sigma_h = .4$ m

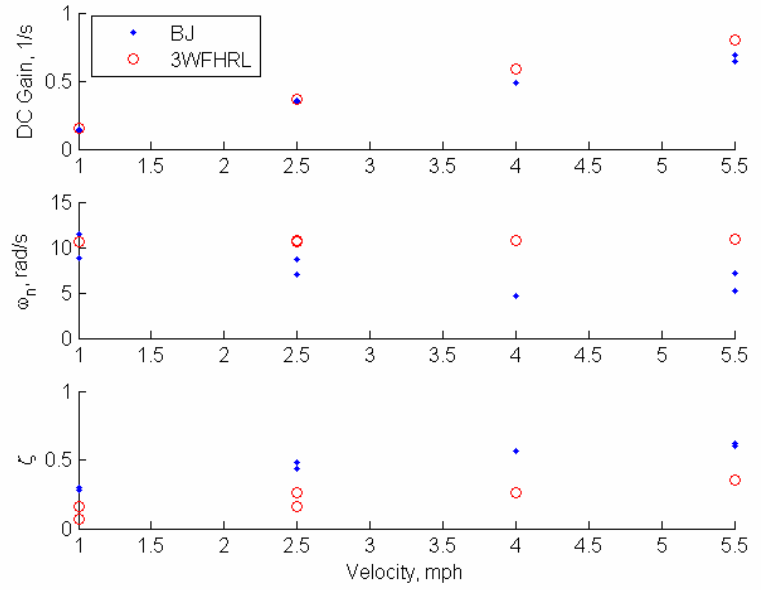

Figure 4.25: DC Gain, Natural Frequency, and Damping Ratio for the Bedder out of the Ground on the 8520, $\sigma_f = .37$ m, $\sigma_h = .4$ m

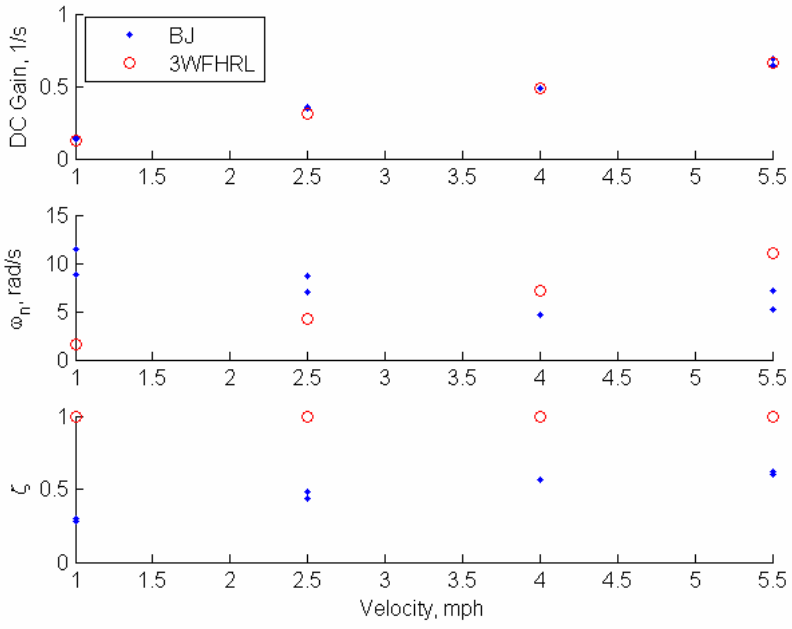

Figure 4.26: DC Gain, Natural Frequency, and Damping Ratio for the Cultivator on the 8520, $\sigma_f = .37$ m, $\sigma_h = .4$ m

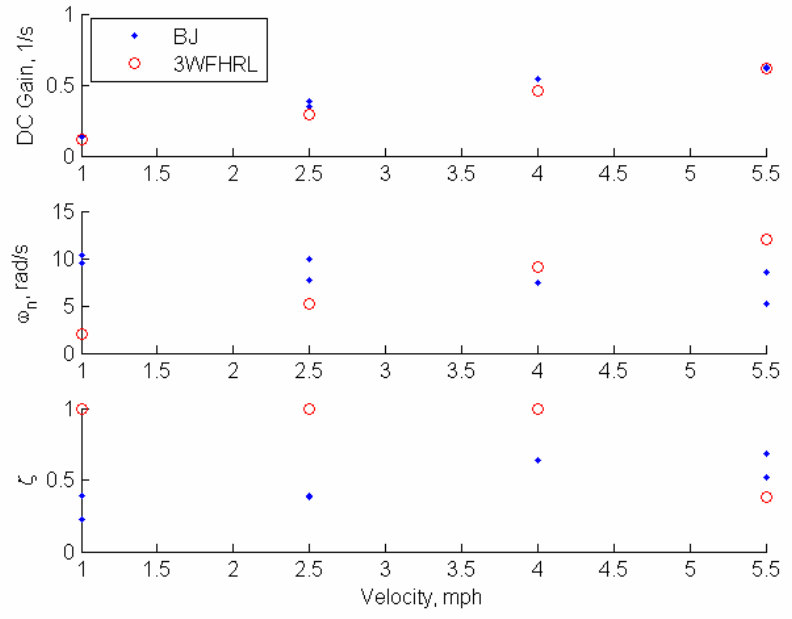

Figure 4.27: DC Gain, Natural Frequency, and Damping Ratio for the Bedder on the 8520, $\sigma_f = .37$ m, $\sigma_h = .4$ m

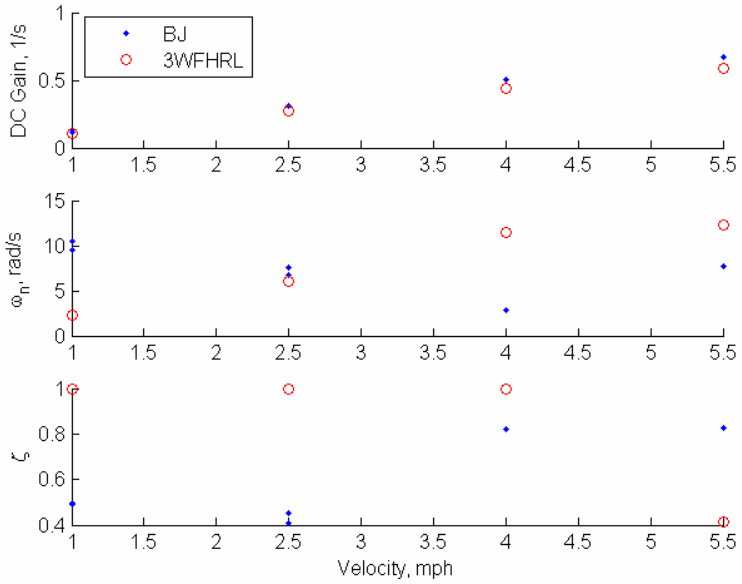

Figure 4.28: DC Gain, Natural Frequency, and Damping Ratio for the 5 Shank Ripper at 10” depth on the 8520, $\sigma_f = .37$ m, $\sigma_h = .4$ m

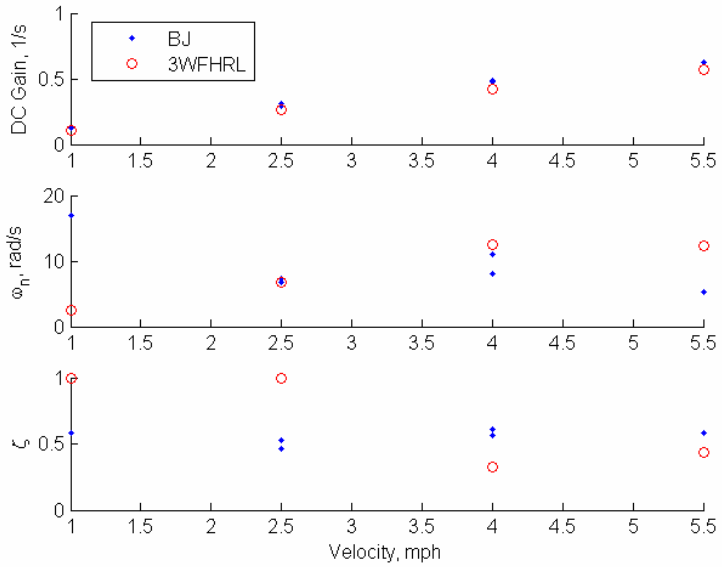

Figure 4.29: DC Gain, Natural Frequency, and Damping Ratio for the 5 Shank Ripper at 15” depth on the 8520, $\sigma_f = .37$ m, $\sigma_h = .4$ m

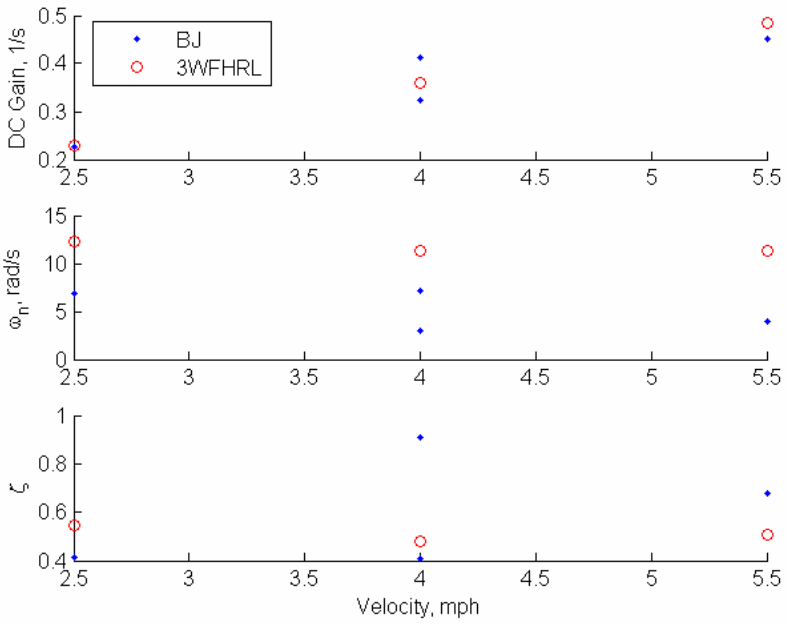

Figure 4.30: DC Gain, Natural Frequency, and Damping Ratio for the 5 Shank Ripper at 20" depth on the 8520, $\sigma_f = .37$ m, $\sigma_h = .4$ m

4.5 Conclusions

In this chapter, steady state data were used to solve for the empirical DC gains of the tractor on a number of implements at a variety of depths and speeds. A minimization function was used to find $C_{\alpha h}$ for each implement at each depth. Dynamic chirp data was used to find the ETFE estimates of each data set, and then fourth order Box Jenkins models were fitted to the ETFE's. The Box Jenkins models were characterized and the DC gains, natural frequencies, and damping ratios were plotted for each implement and depth. Initial values for the front and hitch relaxation lengths were found to be inadequate in modeling the tractor. Therefore, values of front and hitch relaxation lengths were

selected that produced similar damping characteristics as the Box Jenkins models and that also gave the least RMS error values when compared in a dynamic yaw rate tracking scenario as seen in Chapter 2. The values for the front and hitch relaxation lengths were found to be $\sigma_f = .37$ m and $\sigma_h = .4$ m, and the values of $C_{\alpha h}$ for the various implements ranged from 0 N/deg to 3385 N/deg.

CHAPTER 5

MODELING OF FOUR-WHEEL DRIVE EFFECTS

5.1 Introduction

A tractor's towing ability is greatly increased by the addition of a driven front axle. However, since the front axle is usually the steered axle, traction forces affect the tractor's yaw dynamics. In this chapter, a lateral model is derived which takes into account the front axle traction forces of a four-wheel drive tractor. Data has been collected on a tractor both with 4WD on and off. The difference in the respective yaw rates is shown.

5.2 Modeling Front Axle Drive Forces

This section derives the "3-wheeled" Bicycle Model where the four-wheel drive traction forces are not ignored and takes up where Chapter 2 left off. The FBD for the "3-wheeled" Bicycle Model with four-wheel drive traction forces of Figure 2.2 is shown again below as Figure 5.1. The "3-wheeled" Bicycle Model with four-wheel drive traction forces is now termed the "3-wheeled" 4-WD Bicycle Model (3W4BM).

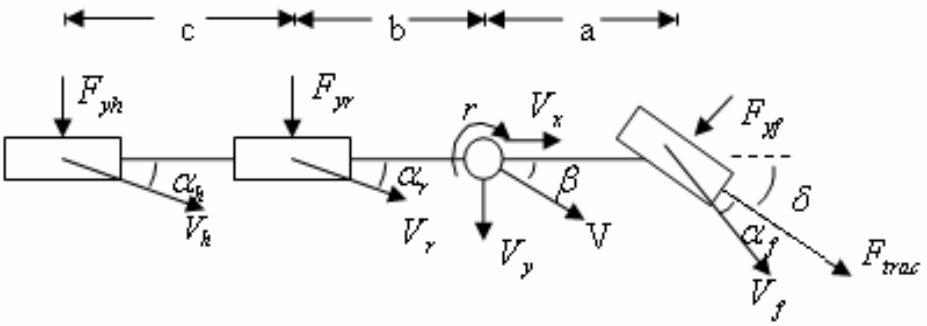

Figure 5.1: "3-wheeled" 4-WD Bicycle Model Schematic

Summing the forces in the Y and Z axes of the tractor yields Equations (5.1-5.2).

$$\sum F_y = m \cdot a_y = F_{yh} + F_{yr} + F_{yf} \cdot \cos(\delta) + F_{trac} \cdot \sin(\delta) = m\dot{V}_y + m \cdot V \cdot r \cdot \cos(\beta) \quad (5.1)$$

$$\sum M_{CG} = F_{yf} \cdot \cos(\delta) \cdot a - F_{yh} \cdot (b+c) - F_{yr} \cdot b + F_{trac} \cdot \sin(\delta) \cdot a = I_z \cdot \dot{r} \quad (5.2)$$

The small β assumption causes $\cos(\beta) \approx 1$ and assuming small steering angles allows $\cos(\delta) \approx 1$, so that Equations (5.1-5.2) become Equations (5.3-5.4).

$$m\dot{V}_y + m \cdot V \cdot r = m \cdot a_y = F_{yh} + F_{yr} + F_{yf} + F_{trac} \cdot \delta \quad (5.3)$$

$$I_z \cdot \dot{r} = F_{yf} \cdot a - F_{yr} \cdot b - F_{yh} \cdot (b+c) + F_{trac} \cdot \delta \cdot a \quad (5.4)$$

F_{trac} is defined below in Equation (5.5)

$$F_{trac} = C_x \cdot \%Slip \quad (5.5)$$

Where $\%Slip$ is the percent of slip along the longitudinal axis of the tire and C_x is the longitudinal tire stiffness. C_x is dependent on the particular tire design, but not on tire-soil conditions. A diagram of the tire forces can be seen in Figure 5.2 below. The tractive

forces of a tire are highly dependent on the tire-soil interaction which affects the $\%Slip$. It should be noted that Equation (5.5) is valid only below a slip of approximately 10%.

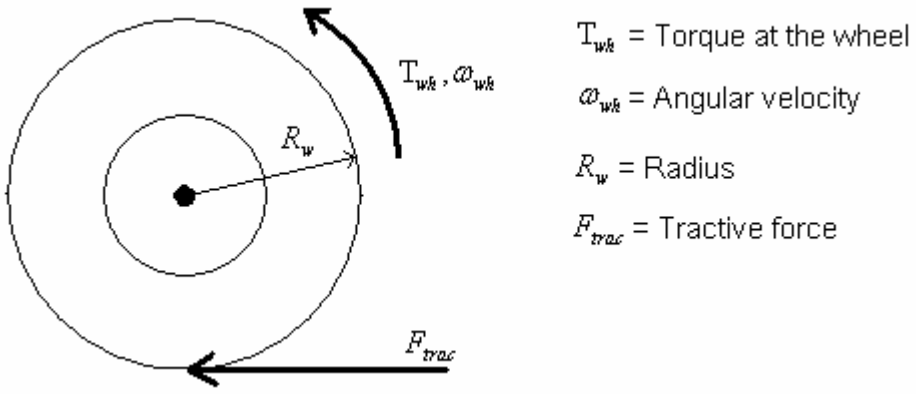

Figure 5.2: Tire Force Schematic

Substituting Equations (2.33-2.35) into Equations (5.3-5.4) yields Equations (5.5-5.6).

$$m\dot{V}_y + m \cdot V \cdot r = -C_{\alpha h} \cdot \alpha_h - C_{\alpha r} \cdot \alpha_r - C_{\alpha f} \cdot \alpha_f + F_{trac} \cdot \delta \tag{5.5}$$

$$I_z \cdot \dot{r} = C_{\alpha h} \cdot \alpha_h \cdot (b+c) + C_{\alpha r} \cdot \alpha_r \cdot b - C_{\alpha f} \cdot \alpha_f \cdot a + F_{trac} \cdot \delta \cdot a \tag{5.6}$$

Using the small β assumption to say $V_x \approx V$, substituting Equations (2.13-2.15) into Equations (5.5-5.6) and organizing the resulting equations into state space form yields Equations (5.7-5.8).

$$\dot{V}_y = r \cdot \left(\frac{C_{\alpha h} \cdot (b+c) + C_{\alpha r} \cdot b - C_{\alpha f} \cdot a}{m \cdot V} - V \right) + V_y \cdot \left(\frac{-\left(C_{\alpha h} + C_{\alpha r} + C_{\alpha f}\right)}{m \cdot V} \right) + \left(\frac{F_{trac} + C_{\alpha f}}{m} \right) \cdot \delta \tag{5.7}$$

$$\dot{r} = r \cdot \left(\frac{-\left(C_{\alpha h} \cdot (b+c)^2 + C_{\alpha r} \cdot b^2 + C_{\alpha f} \cdot a^2\right)}{I_z \cdot V} \right) + V_y \cdot \left(\frac{C_{\alpha h} \cdot (b+c) + C_{\alpha r} \cdot b - C_{\alpha f} \cdot a}{I_z \cdot V} \right) + \left(\frac{F_{trac} \cdot a + C_{\alpha f} \cdot a}{I_z} \right) \cdot \delta \tag{5.8}$$

Rearranging Equations (5.7-5.8) and assuming F_{trac} is a steady state value yields the state-space form of the "3-wheeled" 4-WD Bicycle Model, shown in Equation (5.9).

$$\begin{bmatrix} \dot{V}_y \\ \dot{r} \end{bmatrix} = \begin{bmatrix} \frac{-\left(C_{\alpha h} + C_{\alpha r} + C_{\alpha f}\right)}{m \cdot V} & \frac{C_{\alpha h} \cdot (b+c) + C_{\alpha r} \cdot b - C_{\alpha f} \cdot a}{m \cdot V} - V \\ \frac{C_{\alpha h} \cdot (b+c) + C_{\alpha r} \cdot b - C_{\alpha f} \cdot a}{I_z \cdot V} & \frac{-\left(C_{\alpha h} \cdot (b+c)^2 + C_{\alpha r} \cdot b^2 + C_{\alpha f} \cdot a^2\right)}{I_z \cdot V} \end{bmatrix} \cdot \begin{bmatrix} V_y \\ r \end{bmatrix} + \begin{bmatrix} \frac{F_{trac} + C_{\alpha f}}{m} \\ \frac{F_{trac} \cdot a + C_{\alpha f} \cdot a}{I_z} \end{bmatrix} \cdot \delta \qquad (5.9)$$

The transfer function form of Equation (5.9) is shown in Equation (5.10), below.

$$\frac{r(s)}{\delta(s)} = \frac{m \cdot V \cdot \left(F_{trac} \cdot a + C_{\alpha f} \cdot a\right) \cdot s + \left(F_{trac} + C_{\alpha f}\right) \cdot \left(a \cdot \left(C_{\alpha h} + C_{\alpha r} + C_{\alpha f}\right) + \left(C_{\alpha h} \cdot (b+c) + C_{\alpha r} \cdot b - C_{\alpha f} \cdot a\right)\right)}{Den} \qquad (5.10)$$

Where

$$\begin{aligned} Den = {} & I_z \cdot m \cdot V \cdot s^2 + \left(\left(C_{\alpha h} + C_{\alpha r} + C_{\alpha f}\right) + m \cdot \left(C_{\alpha h} \cdot (b+c)^2 + C_{\alpha r} \cdot b^2 + C_{\alpha f} \cdot a^2\right)\right) \cdot s + \\ & \left(C_{\alpha h} + C_{\alpha r} + C_{\alpha f}\right) \cdot \left(C_{\alpha h} \cdot (b+c)^2 + C_{\alpha r} \cdot b^2 + C_{\alpha f} \cdot a^2\right) + \\ & m \cdot V \cdot \left(C_{\alpha h} \cdot (b+c) + C_{\alpha r} \cdot b - C_{\alpha f} \cdot a\right) + \left(C_{\alpha h} \cdot (b+c) + C_{\alpha r} \cdot b - C_{\alpha f} \cdot a\right)^2 \end{aligned} \qquad (5.11)$$

5.3 Effects of Using Four-Wheel Drive on Yaw Rate

Data from a typical setup using a hitched implement is recorded with and without using the four-wheel drive to determine the effect on yaw rate of the traction forces in nominal conditions. Data was taken on the 8420 with a six shank Paratil at depths of 9, 13, and 17 inches at speeds of 4 mph and 1.5 mph at a depth of 17 inches. The Paratil can be seen in Figure 5.3.

Figure 5.3: 6 Shank Paratil Attached to the 8420

Figure 5.4 shows a typical data set where yaw rate has been plotted vs. steering angle at the wheel. Figure 5.4 has been fitted with a linear fit and is representative of the other data runs at the respective depths and speeds. Figure 5.5 shows the results of comparing yaw rates at 4 mph and 9 inches of depth for both the 4WD on and off. The blue shaded area represents the difference in yaw rate between the two options. A summary of the difference in yaw rate slope vs. steering angle is given in Table 5.1. There is approximately an 8.8% difference in yaw rate between having the 4WD on vs. off at 9 inches depth and 4 mph with the Paratil. Figure 5.6 compares yaw rates with and without 4WD on the Paratil at a depth of 13 inches and a speed of 4mph. There is a difference of 20.6% between the respective yaw rates. Figure 5.7 compares yaw rates at a

depth of 17 inches and a speed of 1.5 mph. The forward velocity on this data set was traction limited by the tractor in 2WD mode. The difference in yaw rates for 17 inches of depth is 15.4%. Intuition would lead one to think that there should be more difference in yaw rates as the depth increases such as for the depths of 9 and 13 inches. One reason for 17 inches being a 15.4% difference and 13 inches being a 20.6% difference is that the velocity at 17 inches is only 1.5 mph instead of 4 mph.

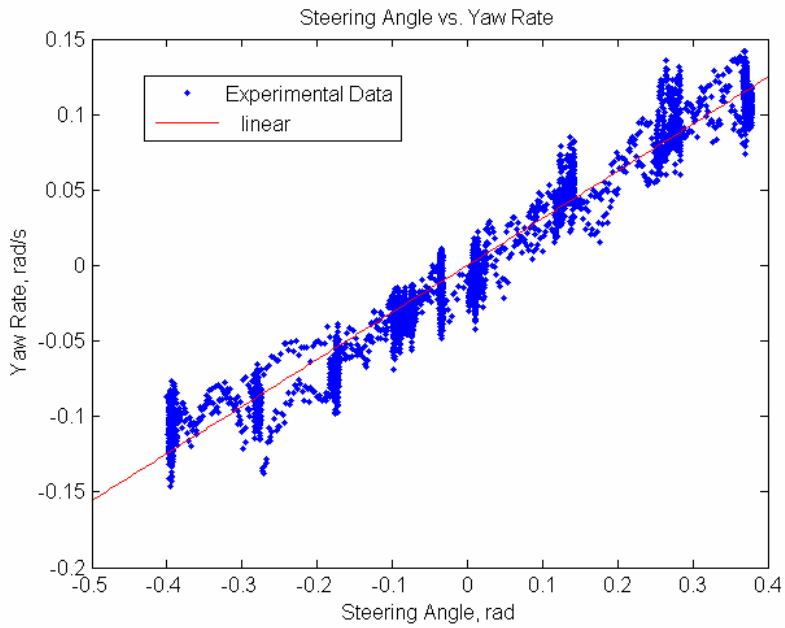

Figure 5.4: Representative Individual Data Run with Linear Fit, 2WD 9" Depth

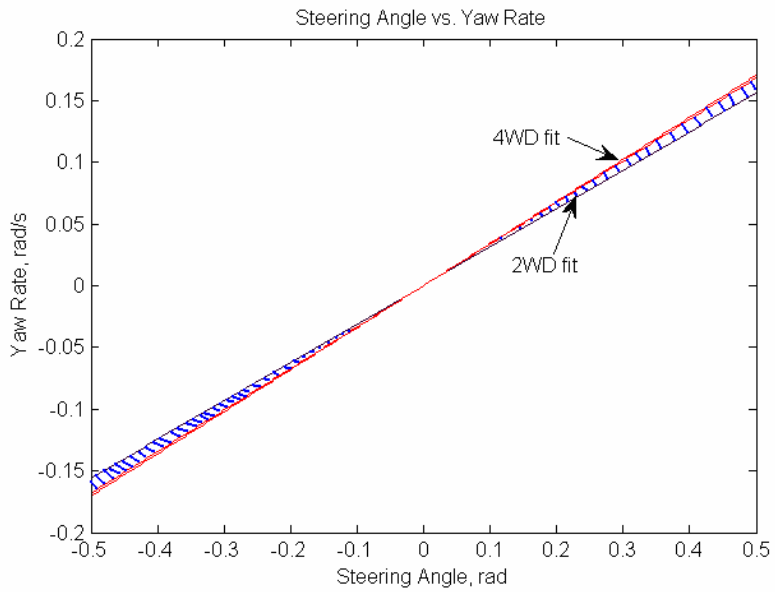

Figure 5.5: Comparison of 4WD vs. 2WD Yaw Rates per Steering Angle, 9" Depth, 4 mph

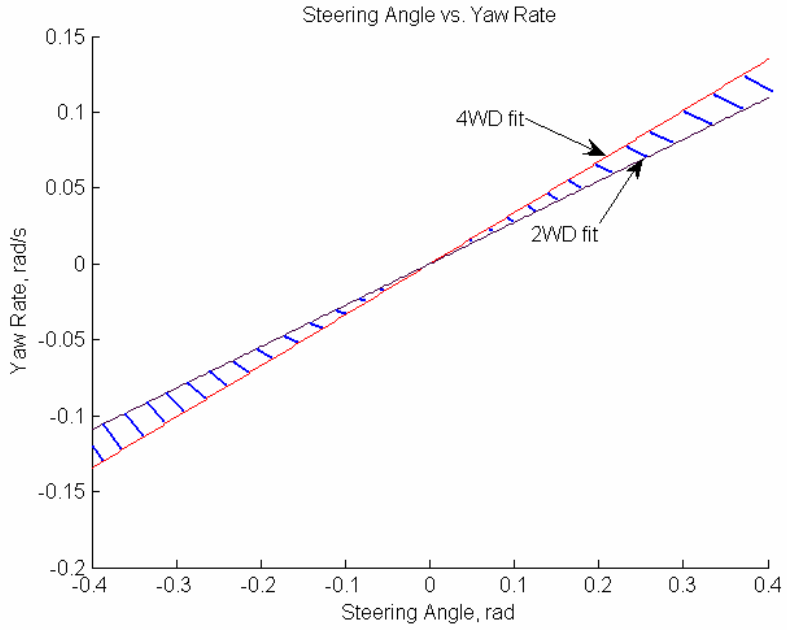

Figure 5.6: Comparison of 4WD vs. 2WD Yaw Rates per Steering Angle, 13" Depth, 4 mph

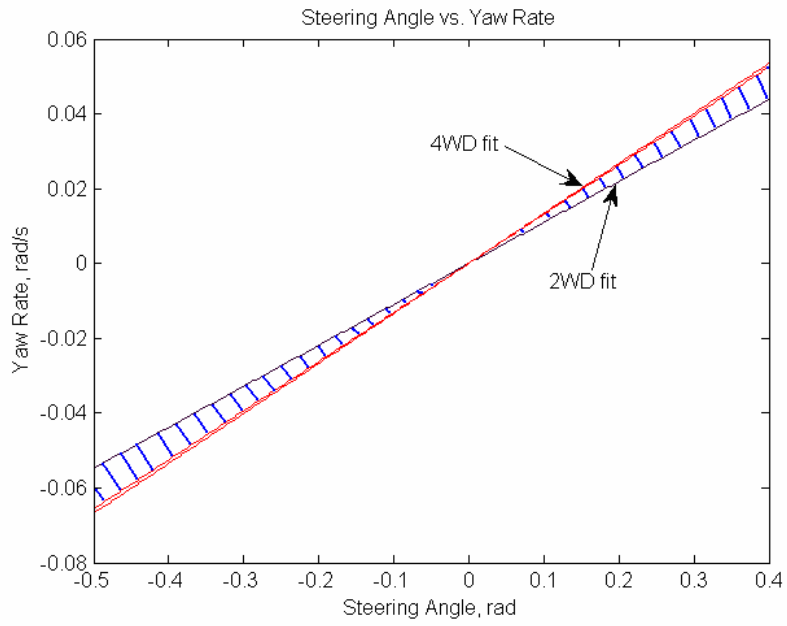

Figure 5.7: Comparison of 4WD vs. 2WD Yaw Rates per Steering Angle, 17" Depth, 1.5 mph

Table 5.1: Values from 4WD Analysis

Depth, inches	Speed, mph	Yaw Rate Slope, 1/s	% Difference in 4WD ON vs. OFF	% Diff/ Velocity
9	4	.34 4WD .31 2WD	8.8	2.20
13	4	.34 4WD .27 2WD	20.6	5.15
17	1.5	.13 4WD .11 2WD	15.4	10.27

5.4 Conclusions

A model which takes into account the front axle traction forces has been developed and termed the “3-wheeled” 4-WD Bicycle Model. Data were collected on a Paratil at three depths and two speeds, both with and without the four-wheel drive. This data shows that under typical conditions, using four-wheel drive does significantly affect the yaw dynamics of the tractor. Using four-wheel drive provided an increase in yaw rate from 9-21%, depending on the depth and speed.

CHAPTER 6

CONCLUSIONS

6.1 Summary

A number of mathematical models for the dynamics of a tractor with a hitched implement has been developed and compared for accuracy. A model has been developed which has the ability to capture changing implement conditions through a hitch cornering stiffness term. The model used to capture the hitched implement forces has been verified to be reasonably correct. The hitch cornering stiffness term has been solved for through a minimization for a variety of implements at varying depths. A model has also been developed which can take into account the effects of using four-wheel drive on the yaw dynamics. A summary of each chapter given in this thesis is provided below.

In Chapter 2, a general diagram is shown from which many tractor vehicle models can be developed. The “3-wheeled” Bicycle Model is developed which can account for changing hitched implement conditions. A model is also developed where front and hitch relaxation lengths are added to the “3-wheeled” Bicycle Model (FHRL Model). Also a number of models used in previous research are derived for a comparison. It is shown that the FHRL Model breaks down into the “3-wheeled” Bicycle Model under steady state conditions. Additionally, under steady state and dynamic steering maneuvers, the FHRL model provides the most accurate yaw rate tracking ability.

In Chapter 3, the Linear Tire Model used in modeling the hitch forces of the FHRL Model is verified. Analysis of experimental data shows that the lateral hitch force vs. slip angle of the implement is relatively linear and can be represented by the Linear Tire Model.

In Chapter 4, steady state experiments using various implements at various depths are used to derive empirical DC gain data. This empirical DC gain data are used to solve for the hitch cornering stiffness term for the varying implements at their varying depths. It is shown that the trends in the hitch cornering stiffness values behave as expected when related to real world behavior. Dynamic steering experiments taken with the various implements and their varying depths are used to derive empirical system identification models for the implements at each respective depth. The system identification models are used to find the front tire and hitch relaxation lengths of the FHRL Model.

In Chapter 5, a "3-wheeled" 4-WD Bicycle Model is developed which takes into account front axle traction forces in a four-wheel drive tractor. Experimental data show that under typical conditions, using four-wheel drive does significantly affect the yaw dynamics of the tractor. Using four-wheel drive provided an increase in yaw rate from 9-21% for a 6 shank Paratil, depending on depth and speed.

6.2 Recommendations for Future Work

Varying ground conditions such as ground moisture, type and compaction also affect the amount of lateral force an implement generates. These varying conditions need to be studied to find their effect on the implement model. The work in this thesis only

considers hitched implement conditions. Research could also be conducted to include towed implements, articulated tractors, skid steer, and even rear steer tractors.

The four-wheel drive modeling should be researched further. It was shown that using four-wheel drive increases the yaw rate at a given steering angle by a significant amount. It needs to be determined whether this difference in yaw rate is captured by the analytical model. It could be the case where physically using four-wheel drive on the tractor reduces the slip losses enough so that the actual yaw rate and the predicted yaw rate from a non four-wheel drive model match since slip is neglected in the model.

REFERENCES

[1] O'Connor, M., Bell, T., Elkaim, G., and Parkinson, B. "Automatic Steering of Farm Vehicles Using GPS," in *Proc. 3rd Int. Conf. Precision Farming*, June 1996 pp. 767–777.

[2] Rekow, A., *System Identification, Adaptive Control, and Formation Driving of Farm Tractors*, Ph.D. Dissertation, Stanford University, March 2001.

[3] O'Connor, M.L., *Carrier-Phase Differential GPS for Automatic Control of Land Vehicles*, Ph.D. Dissertation, Stanford University, December 1997.

[4] Wong, J.Y. *Theory of Ground Vehicles*. Wiley, New York, 1978.

[5] Ellis, J.R. *Vehicle Dynamics*. London Business Books Ltd., 1969.

[6] Owen, R.H., and Bernard, J.E., "Directional Dynamics of a Tractor-Loader-Backhoe," *Vehicle System Dynamics*, Vol. 11, 1982, pp. 251-265.

[7] Bevly, D. M., Gerdes, J. C., and Parkinson, B., 2002, ''A New Yaw Dynamic Model for Improved High Speed Control of a Farm Tractor,'' *J. Dyn. Syst., Meas., Control*, 124(4), pp. 659–667.

[8] Bell, T., *Precision Robotic Control of Agricultural Vehicles on Realistic Farm Trajectories*, Ph.D. Dissertation, Stanford University, June 1999.

[9] Bevly, D.M., *High Speed, Dead Reckoning, and Towed Implement Control for Automatically Steered Farm Tractors Using GPS*, Ph.D. Dissertation, Stanford University, August 2001.

[10] Feng , L., He, Y., and Zhang, Q., "Dynamic Trajectory Model of a Tractor-Implement System for Automated Navigation Applications," *Proceedings of Automation Technology for Off-road Equipment*, MI, USA, pp.243-254, 2004.

[11] Bukta, A.J., 1998, “Nonlinear Dynamics of Traveling Tractor-Implement System Generated by Free Play in the Linkage,” *J. Japanese Society of Agric. Machinery* 60(4): 45-53.

[12] Gillespie, T., 1992, *Fundamentals of Vehicle Dynamics*, Society of Automotive Engineers, Inc., Warrendale, PA.

[13] Figiola, R.S., Beasley, D.E., *Theory and Design for Mechanical Measurements*, 3rd ed., John Wiley & Sons, Inc., 2000.

[14] Ljung, L., 1987 *System Identification: Theory for the User,* PTR Prentice Hall, Inc., Englewood Cliffs, NJ.

[15] Stengel, R. F., *Optimal Control and Estimation*, Dover Publications, Inc., New York, NY.

[16] Bosch, P. P. J., Klauw, A. C., *Modeling, Identification, and Simulation of Dynamical Systems,* CRC Press, London.

APPENDICES

APPENDIX A

Experimental and Data Acquisition Setup

A.1 Introduction

Appendix A contains information about the physical setup of the experimental tractors used for this research and the data acquisition setup.

A.2 Experimental and Data Acquisition Setup

Two tractors were used to take data. The first tractor, shown in Figure A.1, was a John Deere 8420 with single rear wheels. The second tractor was a Deere 8520 with duals, of which a photo is not shown. Both tractors had the independent front suspension setup.

Figure A.1: Experimental Test Tractor- John Deere 8420

A data acquisition computer was used to record data from an inertial measurement unit (IMU), a steering angle sensor, and GPS data. The data acquisition computer is shown in Figure A.2. It is a Versalogic PC-104 stack computer with a Bobcat processor and data acquisition card enclosed in a Versatainer ruggedized enclosure. The steering angle sensor is shown in Figure A.3 and is a linear potentiometer. The IMU is a 6 DOF

system created from 3 Bosch automotive grade sensors. The Bosch sensors sense both yaw rate and acceleration. Figure A.4 shows how the sensors are arranged in a custom fabricated box to create the IMU which senses yaw, pitch, and roll, and acceleration in each respective axis. The GPS data was gathered on a Starfire GPS unit shown in Figure A.5.

Also, for the experiments done in conjunction with the USDA-ARS National Soil Dynamics Laboratory, a hitch force dynamometer was used. The dynamometer is shown in Figure A.6.

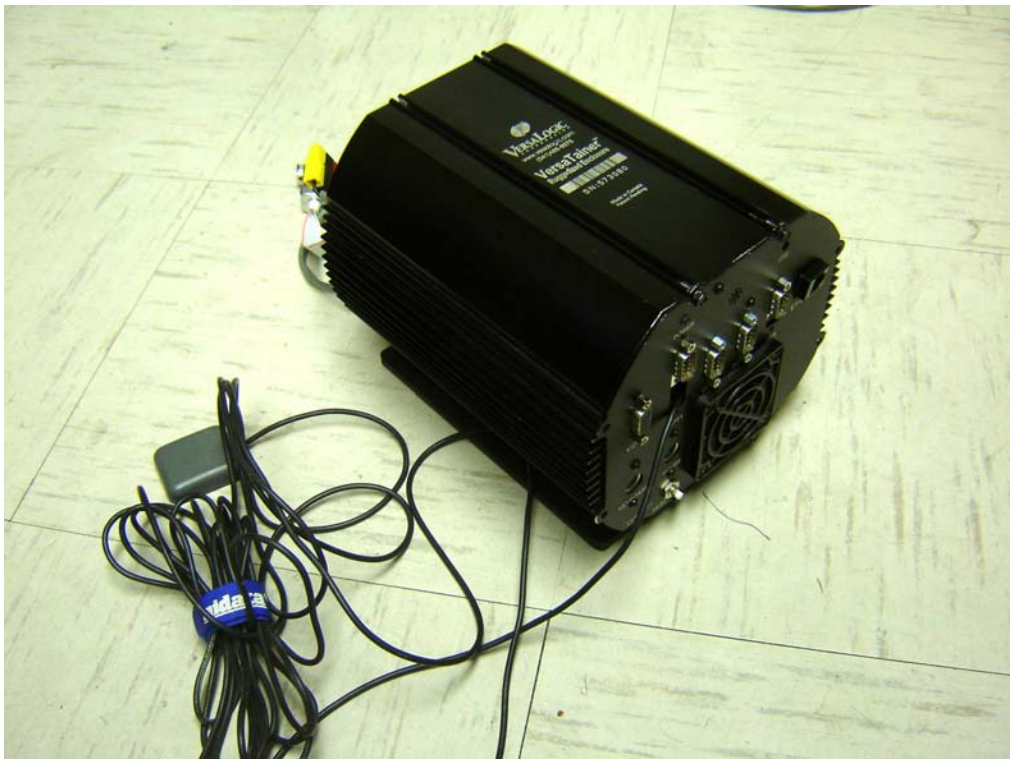

Figure A.2: Versalogic Data Acquisition Computer

Figure A.3: Steering Angle Sensor

Figure A.4: Inertial Measurement Unit

Figure A.5: Starfire GPS Receiver

Figure A.6: Hitch Force Dynamometer

APPENDIX B

Model Parameter Values

B.1 Introduction

Appendix B details the values of the set parameters used in the aforementioned models and also summarizes the values obtained for the parameters whose values were solved for.

B.2 Model Parameter Values

Table B.1: The "3 Wheeled" Bicycle Model Parameters

a	1.00 m
b	2.00 m
c	2.19 m
t	1.20 m
I_z	18500 kgm^2
m	25,000 lb
$C_{\alpha r}$	5000 N/deg (singles, per axle)
$C_{\alpha r}$	10,000 N/deg (duals, per axle)
$C_{\alpha f}$	2,400 N/deg (per axle)
$C_{\alpha h}$	Values shown below in Table B.2
σ_f	.34 m
σ_h	.40 m

The values for *a*, *b*, I_z, $C_{\alpha r}$, and $C_{\alpha f}$ were taken from previous research on a similar setup from Bevly [7]. The values for *c* and *t* were obtained from physical measurements of the tractor. The value for *m* was obtained from the shipping information of the tractor.

Table B.2: $C_{\alpha h}$ Values for all the Implements

Implement	Depth, inches	$C_{\alpha h}$, N/deg
8420, Deere 955 4 Shank Ripper**	6	534.00
8420, Deere 955 4 Shank Ripper**	12	937.00
8420, Deere 955 4 Shank Ripper**	18	1647.00
8420, 4 Shank Ripper	4	451.65
8420, 4 Shank Ripper	8	1002.80
8420, 4 Shank Ripper	12	1719.30
8520, Bedder Out of Gnd	0	0.98 ~ 0.00
8520, Cultivator	9	639.83
8520, Bedder	9	951.24
8520, 5 Shank Ripper	10	887.33
8520, 5 Shank Ripper	15	1025.00
8520, 5 Shank Ripper	20	3385.30

**Note: These values were obtained in a different manner from the rest.

The $C_{\alpha h}$ was determined directly from the F_{yh} vs. α_h plot instead of a minimization based on empirically determined DC gains.